# REPORT DOCUMENTATION PAGE

Form Approved
OMB No 0704-0188

| 1. AGENCY USE ONLY (Leave blank) | 2. REPORT DATE | 3. REPORT TYPE AND DATES COVERED |
|---|---|---|
| | May 10, 1996 | 1/15/93 – 3/15/96 |

**4. TITLE AND SUBTITLE**

PROCESSING AND PROPERTIES OF TOUGH SILICIDES

**5. FUNDING NUMBERS**

AFOSR F49620-93-10092

**6. AUTHOR(S)**

PROFESSOR JOHN J. LEWANDOWSKI
PROFESSOR ROBERT M. AIKIN, JR.

AFOSR-TR-96 97

GG43

**7. PERFORMING ORGANIZATION NAME(S) AND ADDRESS(ES)**

PROFESSOR JOHN J. LEWANDOWSKI
DEPT. MATL'S SCI. AND ENG.
CASE WESTERN RESERVE UNIV.
CLEVELAND, OHIO    44106

**9. SPONSORING/MONITORING AGENCY NAME(S) AND ADDRESS(ES)**

DEPARTMENT OF THE AIR FORCE
AIR FORCE OFFICE OF SCIENTIFIC RESEARCH
BOLLING AIR FORCE BASE,    DC    20332-6488

NA

**10. SPONSORING/MONITORING AGENCY REPORT NUMBER**

**11. SUPPLEMENTARY NOTES**

THE VIEWS, OPINIONS AND/OR FINDINGS CONTAINED IN THIS REPORT ARE THOSE
OF THE AUTHOR AND SHOULD NOT BE CONSTRUED AS AN OFFICIAL DEPARTMENT OF
AIR FORCE POSITION, OR DECISION, UNLESS SO DESIGNATED ELSEWHERE.

**12a. DISTRIBUTION/AVAILABILITY STATEMENT**

APPROVED FOR PUBLIC RELEASE: DISTRIBUTION
        UNLIMITED

**12b. DISTRIBUTION CODE**

**13. ABSTRACT (Maximum 200 words)**

The processing and properties of tough silicides have been investigated. Vacuum hot pressing was utilized to produce $Nb_5Si_3$/Nb laminates, while the fracture toughness of the laminates was evaluated with the use of a deformation stage situated inside of a SEM. The interface strength in such laminates was systematically varied as was the thickness of the Nb layer in order to determine the effects of such changes on the fracture behavior and toughness of such laminates. The effects of changes in test temperature on the above were also determined. Complementary experiments were conducted on in-situ composites where R-curve behavior was obtained. In addition, the effects of changes in grain size, test temperature, and alloy content, on the cleavage fracture stress and the fracture toughness were determined. The results of these experiments were used to rationalize the fracture behavior of the laminates and in-situ composites.

**14. SUBJECT TERMS**

SILICIDES, LAMINATES, TOUGHNESS, DUCTILE PHASE
TOUGHENING, FRACTURE, CLEAVAGE FRACTURE STRESS

**15. NUMBER OF PAGES**
62

**16. PRICE CODE**

| 17. SECURITY CLASSIFICATION OF REPORT | 18. SECURITY CLASSIFICATION OF THIS PAGE | 19. SECURITY CLASSIFICATION OF ABSTRACT | 20. LIMITATION OF ABSTRACT |
|---|---|---|---|
| UNCLASSIFIED | UNCLASSIFIED | UNCLASSIFIED | UNLIMITED |

1997 0117 161

DTIC QUALITY INSPECTED 1

# Table of Contents

# Summary

While many advanced intermetallic systems possess desirable properties such as high temperature strength and stiffness, these systems typically do not exhibit adequate ductility and toughness at low temperatures(i.e. 298K). In addition, there is a need for the development of advanced processing techniques in order to provide materials in adequate quantities for subsequent use. The successful utilization of these desirable material properties also requires the development of techniques to impart higher toughness without sacrificing strength.

A variety of toughening mechanisms may be utilized to impart toughness in such systems. In brittle matrix systems, toughening may be achieved via the introduction of particles which are either brittle or ductile. In the former case, toughening may occur via crack bowing and/or deflection. The introduction of ductile particles may induce ductile phase toughening. The introduction of the reinforcement imparts some damage tolerance, the details of which are affected by the volume fraction of reinforcement, reinforcement/matrix interface characteristics, and the strength/ductility of the reinforcement. In both cases, it is possible to produce brittle matrix materials which exhibit some degree of damage tolerance. In the composite case, the material actually becomes tougher with an increase in crack length, a phenomenon known as R-curve behavior.

The AFOSR Program at Case Western Reserve University, AFOSR F49620-93-910092, focuses on key issues in the processing and properties of advanced intermetallic composite systems. The period 1/15/93 - 3/15/96 was devoted to the following issues, covered sequentially in the following sections:

       I - Silicide Formation

       II - Nb5Si3 /Nb Laminate Processing, Production, and Properties

       III - Mechanical Behavior of In-Situ Nb5Si3/Nb Composites

       IV - Fracture Toughness and Cleavage Stress of Nb and Nb Alloys

The personnel supported over the period 1/15/93 - 3/15/96 are summarized below:

*Faculty:*

Professor John J. Lewandowski
Professor Robert M. Aikin, Jr.

*Research Associates:*

Dr. Preet M. Singh - Partial Support
Dr. Sunil Patankar- Partial Support
Dr. Chanqi Liu- Partial Support
Dr. Joseph D. Rigney - Partial Support

*Graduate Assistants:*

Mr. Jan Kajuch-Ph.D. Candidate - Full Support
Mr. Joseph D. Rigney -Ph.D. Candidate - Full Support
Mr. John Short- M.S. Candidate - Full Support
Mr. William Zinsser- M.S. Candidate - Full Support
Mr. Anand Samant- M.S. Candidate - Partial Support
Mr. P. Lowhaphandu- M.S. Candidate - Self Support

*Undergraudate Students:*

Mr. Jim Woodring
Mr. John Short

*High School Students:*

Ms. Liz Leeson

The papers published under AFOSR support are summarized below:

1. P.Khadikar, J.D.Rigney, J.J.Lewandowski andK.M.Vedula,*Proc.Mat.Res.Symp.*, (C.C.Koch, et al. eds.), **133,** 523, (1988).

2. J.D.Rigney, P.Khadikar, J.J.Lewandowski andK.M.Vedula,*Proc.Mat.Res.Symp.*, (C.C.Koch, et al. eds.), **133,** 603, (1988).

3. J.J. Lewandowski, D.M. Dimiduk, W. Kerr and M.G. Mendiratta,*Mater. Res. Soc. Symp. Proc.,* **20,** 103, (1988).

4. P. Khadkikar, J.J. Lewandowski and K. M. Vedula, *Metall. Trans. A.,* **20A,** 1247, (1989).

5. J. J. Lewandowski, G. M. Michal, I. Locci and J. D. Rigney,*Proc.Mat.Res.Symp.*, (G. M. Stocks, et al. eds.), **186,** 341, (1990).

6. J. D. Rigney and J. J. Lewandowski, *Proc. Second Int'l Ceramic Sci. and Tech. Congress - Advanced Composite Materials*, (M. D. Sacks, ed.), 519, (1990).

7. M. G. Mendiratta, D. Dimiduk and J. J. Lewandowski, *Metall. Trans A,* **22A,** 1573, (1991).

8. J.D.Rigney, J.J.Lewandowski, L.Matson, M.G.Mendiratta and D. M. Dimiduk, *Proc. Mater. Res. Soc. Symp.*, (D. M. Pope, et al. eds.), **203,** 1001, (1991).

9. J. D. Rigney and J. J. Lewandowski, *Mater. Sci. and Eng.,* **A149,** 143, (1992).

10. J.D.Rigney, P. Singh, and J.J. Lewandowski, *Journal of the Mineral, Metals & Materials Society,* **44,** 36, (1992).

11. J. D. Rigney and J. J. Lewandowski, *Mater. Sci. and Eng.,* **A158,** 31, (1992).

12. J. Kajuch, J.D. Rigney and J.J. Lewandowski,*Mater. Sci. Eng.,* **A155,** 59, (1992).

13. J. D. Rigney and J. J. Lewandowski, *Mater. Sci. and Eng.,* **A149,** 143, (1992).

14. J. D. Rigney and J. J. Lewandowski, *J. of Mater. Sci.,* **28,** 3911, (1993).

15. J. D. Rigney, R. G. Castro and J. J. Lewandowski, *J. of Mater. Sci.,* **28,** 4023, (1993).

16. J. Kajuch, J. Short, C. Liu and J. J. Lewandowski, *Mater. Res. Soc. Symp. Proc.,* **288**, 853, (1993).

17. S. N. Patankar and J. J. Lewandowski, *Mater. Res. Soc. Symp. Proc.,* **288**, 829, (1993).

18. D. Hardwick, P. Martin. S. N. Patankar and J. J. Lewandowski, *ISSI-I*, (R. Darolia, et al. eds.), TMS-AIME, 655, (1993).

19. J. J. Lewandowski, *In-Situ Composites*, (M. Singh and D. Lewis, eds.), TMS, Warrendale, Pa, 159, (1994).

20. J. D. Rigney, J. J. Lewandowski and S. N. Patankar, *Composites Science and Technology*, **52**, 163, (1994).

21. J. Zhang and J. J. Lewandowski, *J. of Mater. Sci.* , **29**, 4022, (1994).

22. J. Short, J. Kajuch and J. J. Lewandowski, *Proc. MRS Symposium-Intermetallic Matrix Composites III* , (J. A. Graves, R. R. Bowman and J. J. Lewandowski, eds.), MRS, Pittsburgh, PA, 285, (1994).

23. J. Kajuch, J. Short and J. J. Lewandowski, *Acta Metall et Materialia*, **43**, 1955, (1995).

24. M. G. Mendiratta, R. Goetz, D. M. Dimiduk and J. J. Lewandowski, *Metall.Trans. A*, **26A**, 1767, (1995).

25. J. D. Rigney and J. J. Lewandowski, *Fatigue and Fracture of Ordered Intermetallic Materials II*, (T. S. Srivatsan, W. O. Soboyejo and R. O. Ritchie, eds.), TMS, Warrendale, PA, 339, (1995).

26. J. D. Rigney and J. J. Lewandowski, *Metall. Trans. A*, **26A**, in press, (1996).

27. A. Samant and J.J. Lewandowski, *Metall. Trans. A*, in review, (1996).

## BOOKS CO-EDITED/PUBLISHED

1. J. J. Lewandowski, ed., *Future Problems in Mechanics and Materials*, UCSD-IMM, San Diego, CA, (1993).

2. R. Darolia, J. J. Lewandowski, C. T. Liu, P. L. Martin, D. B. Miracle and M. V. Nathal, eds., *ISSI-I,* TMS, Warrendale, PA, (1993).

3. J. A. Graves, R. R. Bowman and J. J. Lewandowski, eds., *Intermetallic Matrix Composites III*, MRS, **350**, Pittsburgh, PA, (1994).

4. J. J. Lewandowski and W. H. Hunt, Jr., eds., *Intrinsic and Extrinsic Fracture Mechanisms in Inorganic Composites*, TMS, Warrendale, PA, (1995).

5. J. J. Lewandowski, C. Ward, M.R. Jackson, and W. H. Hunt, Jr., eds., *Layered Materials for Structural Applications*, MRS, **434**, Pitsburgh, PA, in press (1996).

# I  -  Silicide Formation

*Introduction*

Refractory metal silicides are receiving interest as potential candidate materials for replacing nickel and cobalt superalloys in high temperature(1473K - 1873K) applications. While much of the recent work has focused on monolithic $MoSi_2$[1-6] and composites based on this matrix, part of the present work investigates the production of $Nb_5Si_3$ and $Nb_5Si_3$/Nb composites. *In situ* composites of niobium-based silicides discussed in Section III were processed via conventional arc melting and casting processes[7-9] and supplied to CWRU via WRDC. The powder processing approaches discussed presently were used to create the model laminates discussed in Section II in order to aid in analyzing the fracture behavior of the *in situ* processed composites. Mechanical alloying(MA) and reactive sintering(RS) were used in this research for the production of $Nb_5Si_3$ powders and compacts while other work in our laboratory[10,11] has utilized identical technology to produce $MoSi_2$ and other high temperature material systems. The following summarizes various processing schemes for the $Nb_5Si_3$ and $Nb_5Si_3$/Nb composites.

*Mechanical Alloying*

Mechanical alloying is a simple but effective process for the production of intermetallic compounds of high temperature refractory metals. The main advantage as compared to melting and casting processes is in the capability to maintain exact composition(stoichiometry) and flexibility in producing monolithic and composite powders. MA is a non-equilibrium processing technique, analogous to Rapid Solidification. In contrast to the rapid solidification process, the MA process has been defined as a dry, high energy ball milling process that produces composite metal powders with extremely fine microstructures that are often nanocrystalline as shown in our other work[10,11]. Interdispersion of the powders occurs by the repeated cold welding and fracturing process of free powder particles trapped between two colliding steel balls as shown in Figure 1[13]. The force of impact deforms the particles and creates atomically clean surfaces which weld together on contact. To prevent oxidation of these surfaces, the milling operation is carried out in an inert gas atmosphere. Refinement of the structure is approximately a logarithmic function of time and depends on the mechanical energy input into the milling process and the work hardening of the powders being processed[14]. The

6

microstructual refinement continues into the steady state period despite the fact that the hardness saturates and a constant agglomerate particle size distribution is achieved.

Mechanical alloying was carried out in a Spex Model 8000 High Intensity Mixer/Mill with a tungsten carbide vial(38x51mm), 100 g of hardened 52100 steel balls(12mm in diameter) and 10 g of elemental powders with a proper ratio for the formation of $Nb_5Si_3$(Nb-37.5%Si) were weighed(e.g. 8.465 g Nb, 1.535 g Si) and placed into the vial while in an argon filled glove box.

*Continuous Milling*

The continuous milling process was analyzed by milling powders for various milling times as shown in Figure 2. Following classical mechanical alloying theory, the repeated coalescence and fragmentation of the Nb and Si particles creates a layered structure. The inter-layer distance between the Nb and Si atoms decreases with increasing milling time at which point compound formation occurs as shown in Figure 3. Figure 4 shows SEM micrographs of the Nb-Si mixture just before(i.e. 3 hr) and just after(i.e. 3.25 hr) $Nb_5Si_3$ formation.

*Interrupted Milling*

Kumar and his co-workers were the first to study the mechanism of MA in the Group V transition metal/silicon systems and the "interrupted process"[15]. In order to study the progress of mechanical alloying, the ball mill was stopped periodically and cooled to room temperature in order to enable removal of small amounts of the powder for analysis. This "interrupted process" resulted in the formation of $Nb_5Si_3$ in 75 minutes while milling for 73 minutes and cooling to room temperature produced elemental Nb and Si. Whittenberger, in his analysis of the solid state processing of high temperature alloys and composites[16] believes that "enhanced diffusivity" plays a major role in the alloying process. Schaeffer and McCormick studied the mechanism of compound formation in the "interrupted process" in several systems with the conclusion that room temperature "enhanced diffusivity" facilitates the exothermic reaction which occurs almost instantaneously after milling is resumed[17].

Differential Thermal Analysis(DTA), X-ray Diffraction and Scanning and Transmission electron microscopy were utilized to determine the kinetic model for silicide formation. In combination with the continuous milling results, the research provides a comprehensive analysis of the mechanism of silicide formation by mechanical alloying.

A Netzsch STA 429/409 Differential Thermal Analyzer at NASA Lewis Research Laboratories and a modified DTA unit built at Case Western Reserve University were used

7

to determine the critical and onset reaction temperatures on prealloyed powders as well as on reacted powders($Nb_5Si_3$). For DTA tests at CWRU, powder samples(2-5g) were cold pressed into small discs and a center hole was drilled for the insertion of a K type thermocouple, while another K type thermocouple was placed in the alumina crucible as a reference. Argon gas was used to prevent powder oxidation during the analysis and post analysis cooling. Some of these sintered samples were crushed and x-rayed to determine the phase evolution during DTA analysis.

Similar to the continuous milling formation of $Nb_5Si_3$, the "interrupted process" proceeds by a self propagating exothermic reaction upon resumption of the milling process[10,18]. Our work has demonstrated that the major variables controlling compound formation are that a minimum milling time of 1 hour and a minimum cooling time of 2 hours are required prior to the resumption milling in order to facilitate compound formation as shown in Figure 5. The following observations were analyzed to determine the reasons for the critical milling time and hold time at room temperature.

Figure 6 shows the microstructural refinement in a Nb-Si agglomerate after MA for 1 hour. Particles within the agglomerate are not uniformly refined, with an average interparticle spacing on the order of 1 $\mu$m although there are areas where the refinement is on a much smaller scale. According to the theory of mechanical alloying, true alloying occurs when the microstructural refinement is no longer visible in an optical microscope, roughly a particle spacing of 0.5 $\mu$m. With regard to the present work, it appears possible that there are small areas where intensive MA energy input promotes Si dissolution in Nb, creating a supersaturated solid solution with respect to its equilibrium solubility at low processing temperatures.(i.e. 600-900K). Upon cooling, $Nb_5Si_3$ particles precipitate from solid solution as expected from the equilibrium diagram. Upon resumption of milling, a self propagating exothermic reaction takes place, due to a large heat of formation release upon growth of the $Nb_5Si_3$ particles.

In order to understand the above phenomena, Differential Thermal Analyses(DTA) were conducted on powders milled for a total time of 1 hour immediately after the milling process was stopped as well as after room temperature "aging" for up to 1000 hours, as shown in the schematic in Figure 7. Figure 8 shows the onset reaction temperature of $Nb_5Si_3$ vs "aging" time at room temperature, with a total temperature differential of less than 9°C. This small reaction temperature drop suggests that although "enhanced diffusivity" occurred, it does not play a significant role in the compound formation in the interrupted process. In order for the reaction to take place, as shown in Figure 9, enhanced diffusivity would have to decrease the critical reaction temperature on the order of 50C. Here the critical reaction temperature is the temperature at which the heat of reaction is large

8

enough to cause a positive increase in the temperature differential between the sample and the reference thermocouple, while the onset temperature is designated as the temperature at which the reaction is self propagating.

TEM electron diffraction of Nb-Si powders milled for 1 hour, in Figure 10, show particles of Nb+Si mixture as well as $Nb_5Si_3$ compound[10]. No other metastable, amorphous, or equilibrium phases were observed.

In summation, it appears most likely that the initiation of the $Nb_5Si_3$ compound reaction in the interrupted milling process occurs via the precipitation of $Nb_5Si_3$ particles upon cooling from the milling temperatures. The most plausible explanation for the precipitation process is the creation of a non-equilibrium supersaturated solid solution of Si in Nb. TEM observations of powders milled for 3 hours failed to show precipitates other than $Nb_5Si_3$, supporting the mechanism of $Nb_5Si_3$ precipitation.


*Reactive Sintering*


Reactive sintering[18,19] provides another means of producing a compound from elemental powders and is generally possible in systems with large negative heats of formation. In this process, blended powders are isostatically cold pressed and are often ignited by torch in air or by an electrical spark in vacuum to start the self propagating exothermic reaction. RS may also occur without such external input provided an element is molten in the reaction zone. Thus, in contrast to the MA process, where alloying is a result of the solid state processes, RS begins to occur at temperatures near the lowest eutectic. MA may be combined with RS through the fact that MA reduces the onset and critical reaction temperatures, as shown in Figure 9. MA and RS also allow $Nb_5Si_3$ composites to be made in-situ by adjusting the volume fraction of Nb.

In order to explore composite formation via these approaches, powder consolidation was accomplished with a vacuum hot press capable of operating at up to 69 MPa pressure and 2573K using graphite dies, rams and resistance heating elements. The general hot pressing scheme is shown schematically in Figure 11. The degassing stage at 1123K for four hours may be particularly important for powders prepared by the MA process, as significant microcracking was observed in compacts not degassed for a sufficient time at this temperature.

Three types of powder batches were produced for the vacuum hot pressing operation. The first utilized mechanically alloyed $Nb_5Si_3$, while the others used either a pre-alloyed Nb-Si mixture or a blended mixture of Nb-Si powders. The MA-$Nb_5Si_3$ was produced by the continuous milling process described above. The pre-alloyed Nb-Si mixture is a

9

Nb-Si mixture that was milled for 2 hours and blended, while the blended mixture was simply a blended mixture of the Nb-Si elemental powders. All of these mixtures were consolidated using the powder consolidation schematic shown in Figure 11. Table 1 summarizes the hot pressing results, while Figure 12 shows the microstructures produced for the various conditions. Both the hot pressed prealloyed $Nb_5Si_3$ and the MA-$Nb_5Si_3$ exhibited average grain sizes of approximately 5 μm, indicating that fine grain sized material can be produced via such approaches. The prealloyed powder contained about 3 volume percent unreacted Nb. The Nb-Si blend exhibited a bimodal grain size distribution with grains of average size 2-3 μm and 15 μm with about 5 volume percent unreacted Nb. Subsequent work has shown that the additional "holes" shown in Figure 12 result from silicide grain pullout during metallographic preparation.

Reactive sintering and hot pressing techniques were also used for the production of $Nb_5Si_3$ composites. MA-$Nb_5Si_3$ and excess Nb(to 30 vol%) were blended in a horizontal roller blender prior to a reactive sintering. Figure 13 shows the resulting microstructure. The microstructure consists of somewhat clustered Nb particles(i.e. light colored phase). The tendency for clustering of Nb particles is probably a result of the blending efficiency. In contrast to compacts obtained from $Nb_5Si_3$ and pre-alloyed Nb-Si, the reactive sintering method provides compacts with very small porosity as evident in Figure 13. It is easily possible to produce graded structures with such processing techniques.

# Silicide Formation References

1. F.D. Gac and J.J. Petrovic, *J. Amer. Cer. Soc.,* **68**, C200, (1985).
2. J.M. Yang and S.M. Jeng, *Mater. Res. Soc Symp. Proc,* **194**, 139, (1990).
3. S.A Maloy, A.H. Heuer, J.J. Lewandowski and J.J. Petrovic, *J. Amer. Ceram. Soc.,* **74**, 2704, (1991).
4. S.A. Maloy, J.J. Lewandowski, A.H. Heuer and J.J. Petrovic, *Mater. Sci and Eng.,* **A155**, 159, (1992).
5. J.D. Cotton, Y.S. Kim and M.J. Kaufman, *Mater. Sci. Eng,* **A144**, 287, (1991).
6. R. Gibala et. al
7. J.J. Lewandowski, D. Dimiduk, W. Kerr, and M.G. Mendiratta, *Mater. Res. Soc. Symp. Proc.* **120**, 103, (1988).
8. M.G. Mendiratta and D.M. Dimiduk, *Mater. Res Soc. Symp. Proc.,* **133**, 441, (1989).
9. M.G. Mendiratta, J.J. Lewandowski, and D.M. Dimiduk, *Metall. Trans. A.,* **22**, 1573, (1991).
10. J. Kajuch, J. Short, Changqi Liu, and J.J. Lewandowski, MRS Paper
11. Sunil Patatankar, J.J. Lewandowski, A.H. Heuer
12. D. Hardwick, P. L. Martin, S. Patankar, and J.J. Lewandowski,
13. P.S. Gilman and J.S. Benjamin, *Annual Rev. Mat. Science,* **13**, 279, (1983).
14. J.S. Benjamin and T.E. Volin, *Metall. Trans.,* **5**, 1929, (1974).
15. K.S. Kumar and S.K. Mannan, *Mater. Res. Soc. Symp. Proc.,* **133**, 415, (1989).
16. J.D. Whittenberger in A.H. Clauer and J.J. deBarbadillo(eds.) *Solid State Powder Processing.,* The Minerals, Metals and Materials Society, Warrendale, PA, 137 1990).
17. G.B. Schaeffer and P.G. McCormick, *Metall. Trans. A,* **22A**, 3019, (1991).
18. J. Kajuch, J.D. Rigney and J.J. Lewandowski, *Mater. Sci and Eng.,* **A155**, 59, (1992).
19. Z.A. Munir and U. Anselm-Tamburini, *Mater. Sci. Rep.,* **3**, 277, (1989).
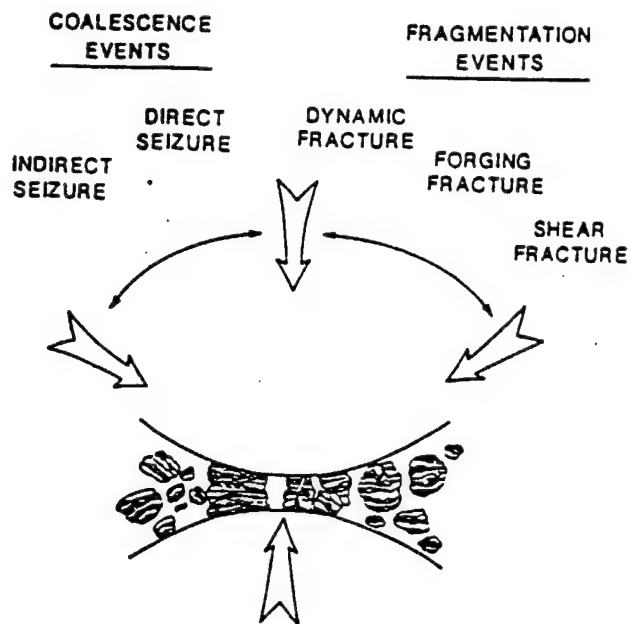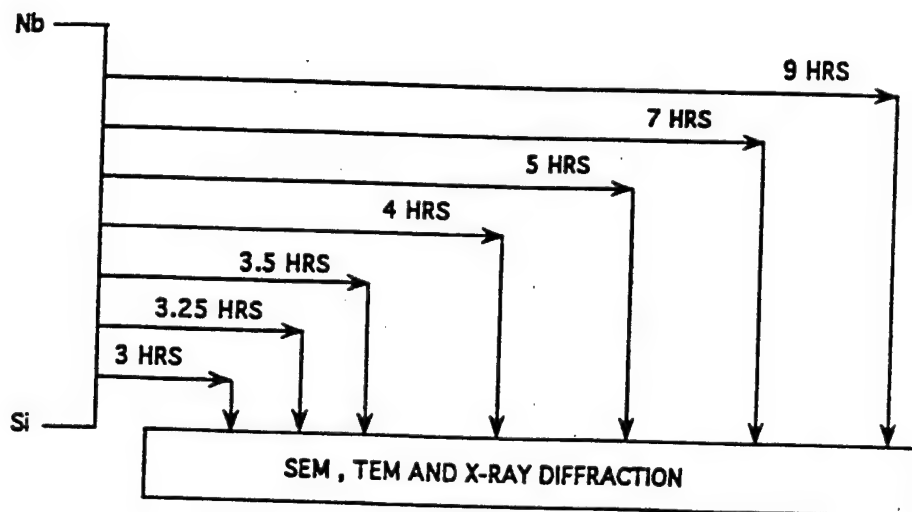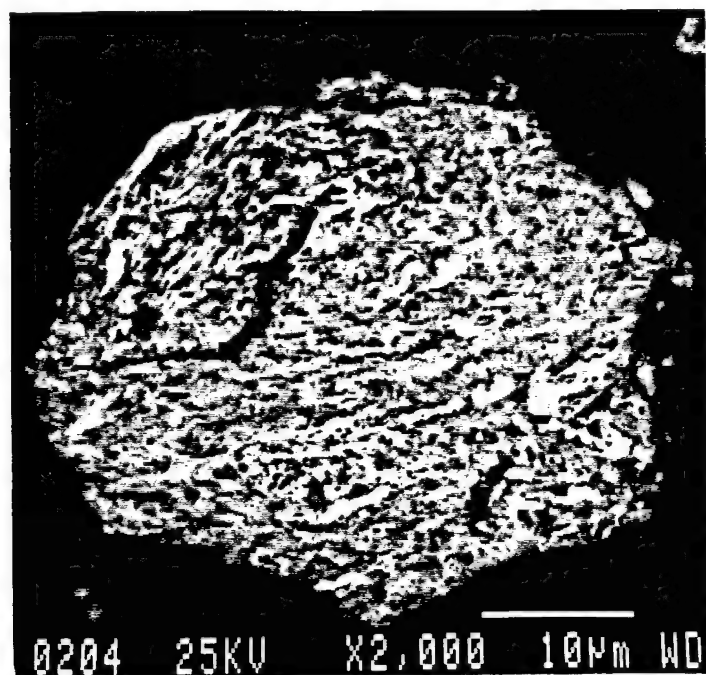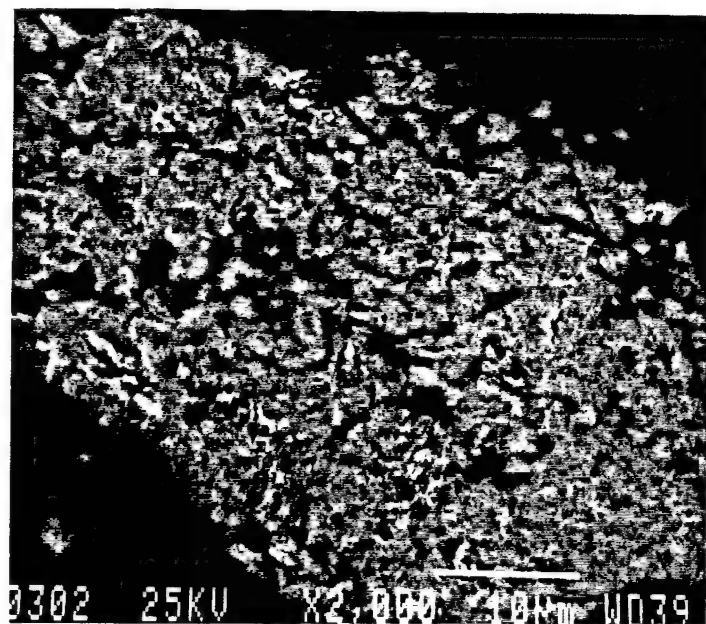
Figure 1 Schematic of Powder Welding Process.



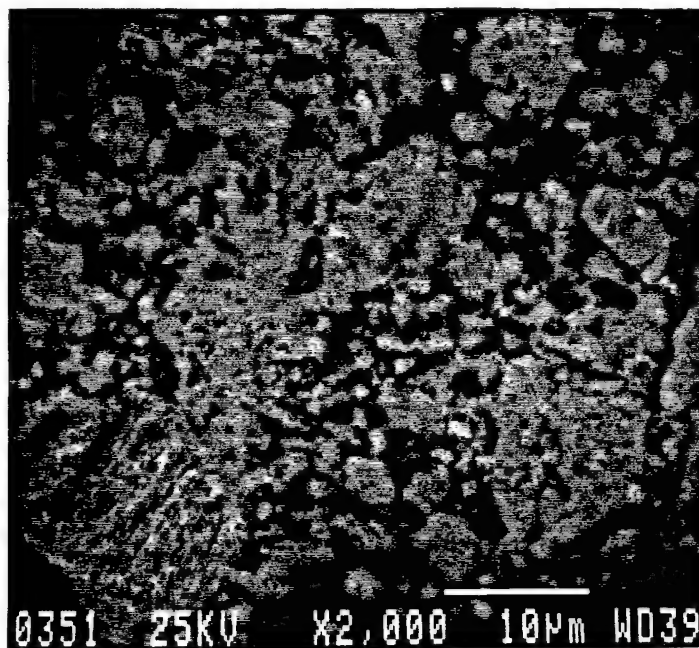Figure 2 Flow Chart of Continuous Milling Process.

1 hr.



2 hrs.

Figure 3 Interparticle Spacing as a function of milling time.
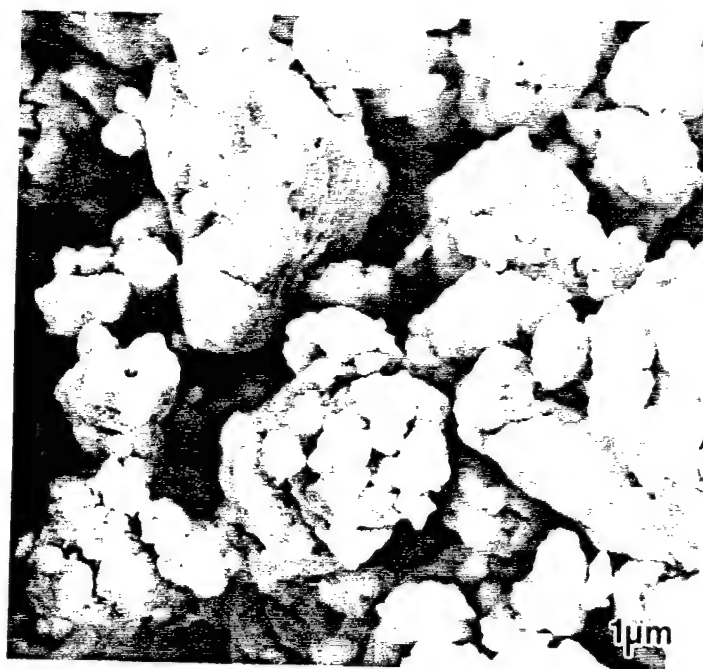
3 hrs.

Figure 3 Interparticle spacing as a function of milling time.

Before reaction(3hrs)                               After reaction(3.25hrs)

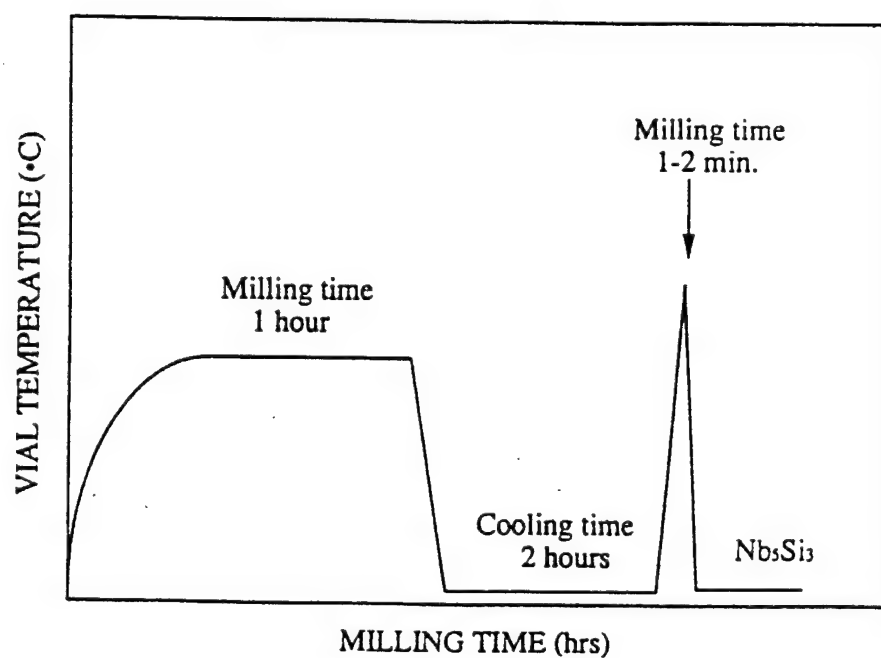Figure 4 SEM Micrograph of Nb-Si mixture milled in the continuous process.



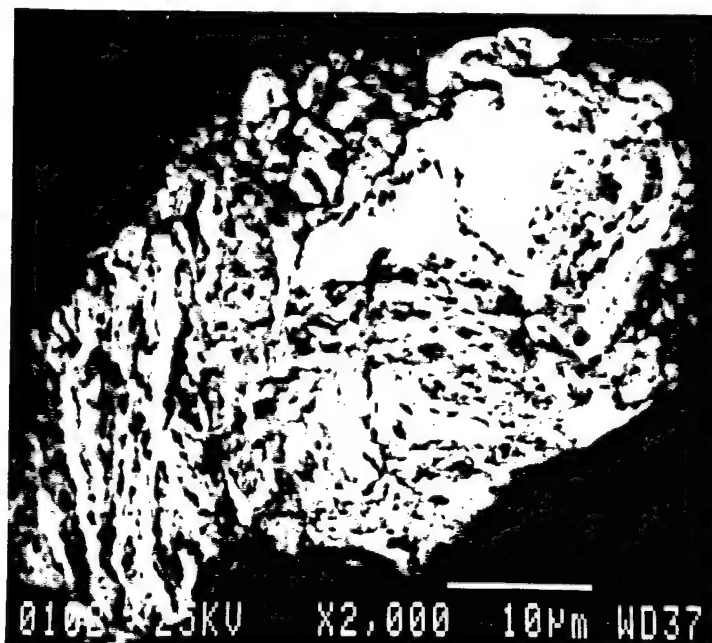Figure 5 Schematic of the Interrupted Milling Process.

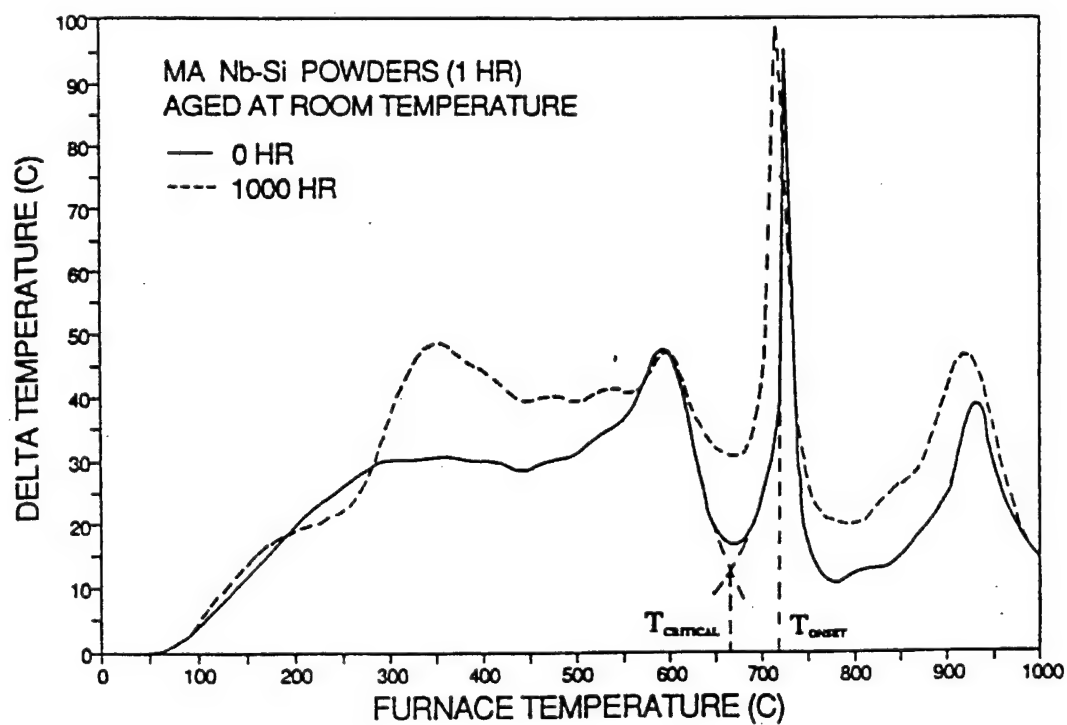Figure 6 SEM micrograph of Nb-Si mixture milled for 1 hr.



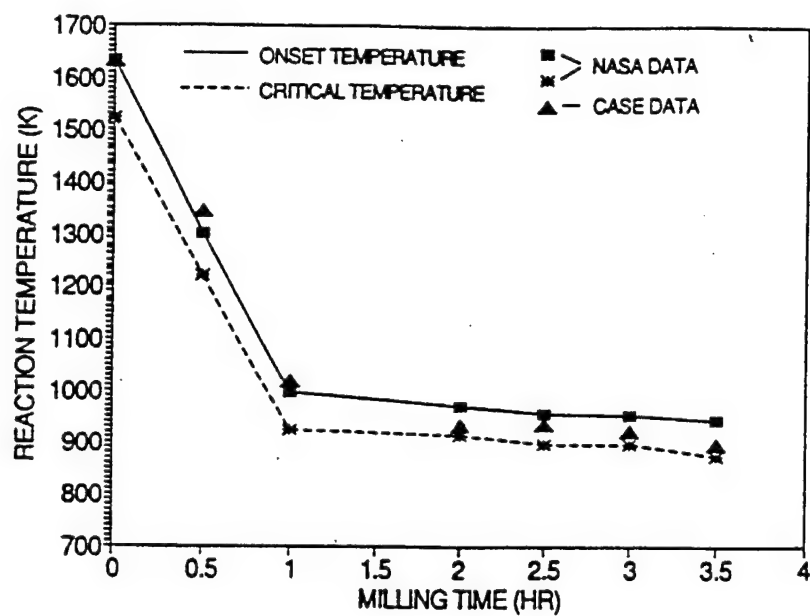Figure 7 DTA trace of MA Nb-Si Powders(1hr) aged at room temperature.

Figure 8 Reaction onset temperature vs. aging time at room temperature.
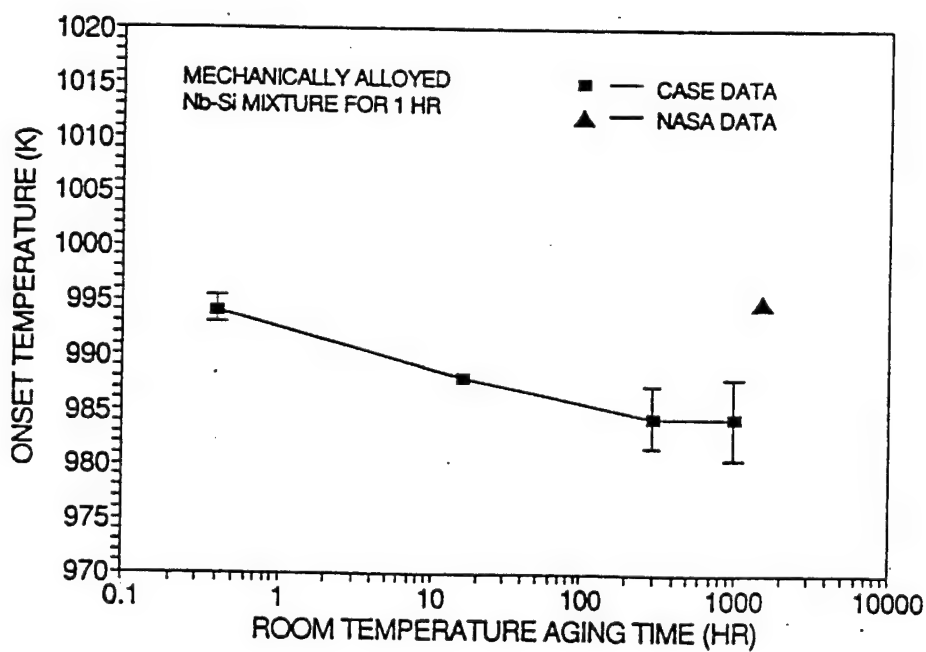


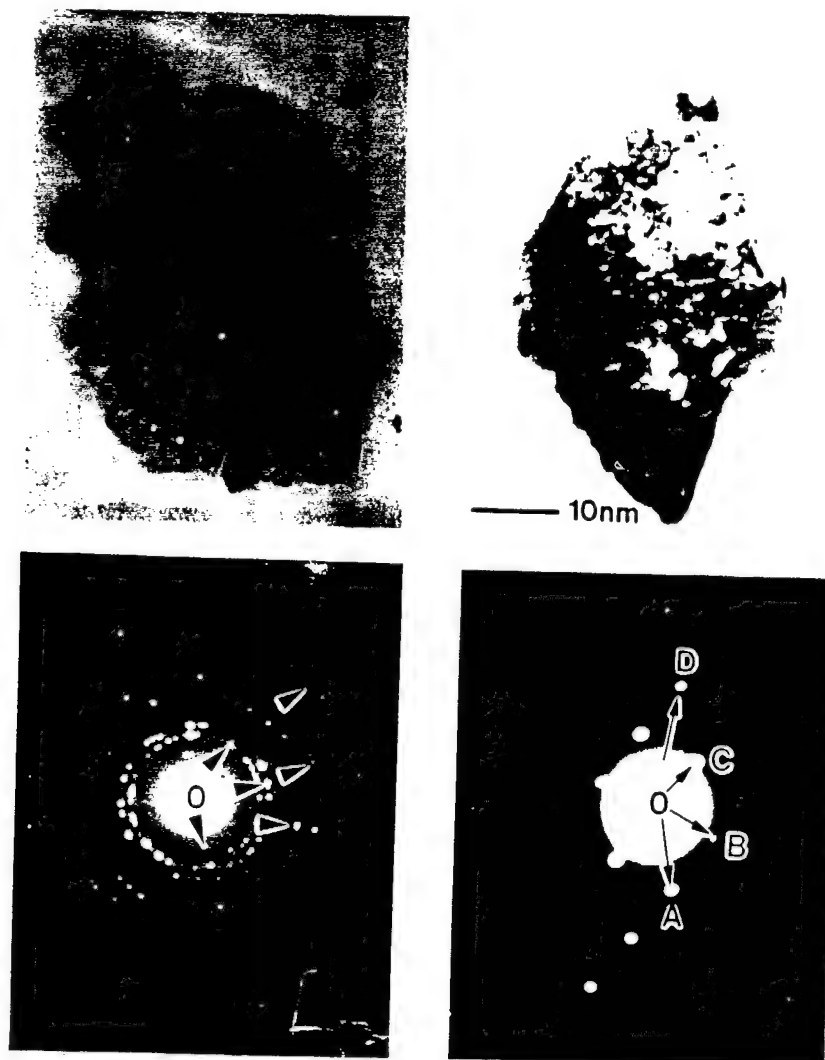Figure 9 Critical and onset reaction temperature vs milling time.

17

Nb + Si mixture                                          α - Nb5Si3

Figure 10 TEM micrographs and diffraction patterns of Nb-Si mixture milled for 3hrs.

CONSOLIDATED POWDERS: • Mechanical alloyed Nb + Si mixture

• Mechanical alloyed Nb₅Si₃

• Blended Nb + Si powders

APPLY PRESSURE
~ 55 MPa

CONSOLIDATION
1600-1700 °C / 1-2 HRS

DEGAS:
850 °C / 1-4 hrs

HEAT-UP
~8°C/min

COOLING
~ 5 °C/min

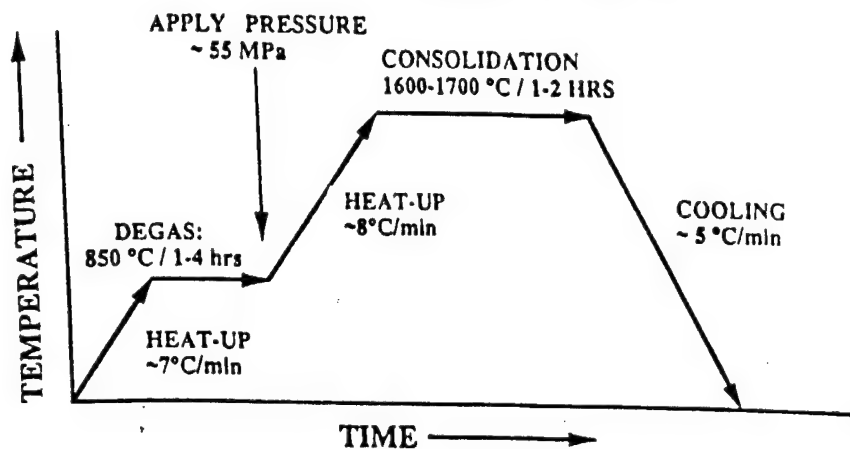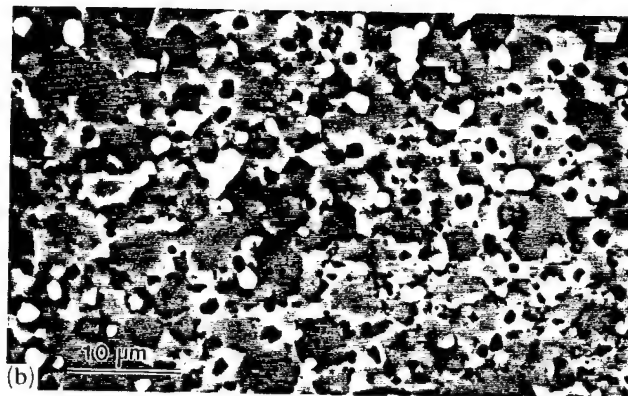HEAT-UP
~7°C/min

TEMPERATURE

TIME

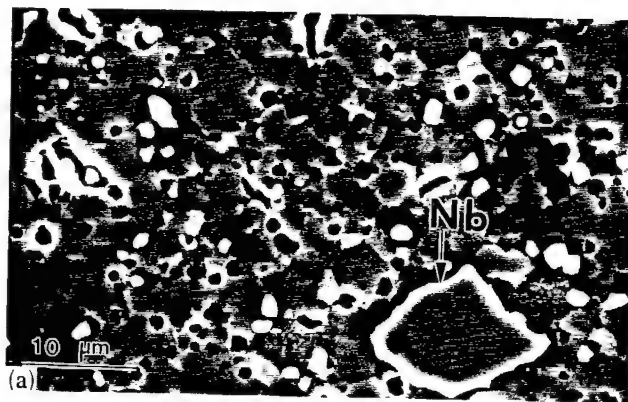Figure 11 Schematic of the powder consolidation process.



Reaction Sintered (2hr milling)

Figure 12 Structures of Hot pressed Nb₅Si₃.

19

Nb5Si3 Powder



Powder Blended in 5:3 ratio(no milling)
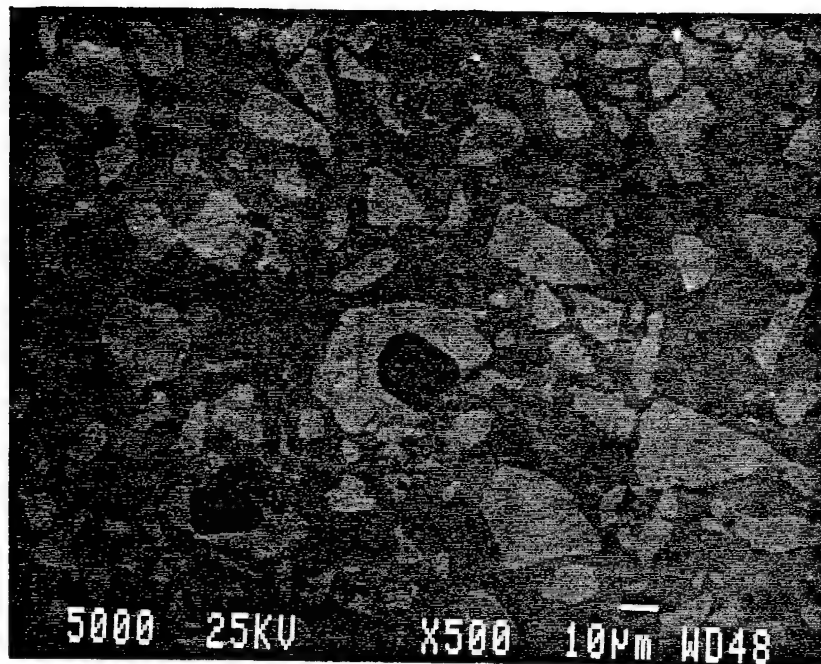
Figure 12 Structures of Hot Pressed Nb5Si3.

Figure 13 SEM Micrograph of Nb5Si3 30 vol% Nb composite.

# II - Laminate Processing and Properties

## Introduction

Extrinsic toughening approaches(i.e. compositing) have been used to increase the toughness of the brittle intermetallic systems[1]. The incorporation of the "ductile phase" or "ductile phase toughening" has emphasized that the degree of toughening depends on several factors including strength, plastic properties, and volume fraction of reinforcement, as well as the work of rupture. The work of rupture is affected by the degree of constraint which, in turn is controlled by reinforcement/matrix strength. Model experiments on the lead/glass system have shown that very high stress can be achieved in constrained ductile ligaments[2]. However, the primary effect of the constraint is to accelerate ductile fracture mechanisms. Ductile to brittle transitions for bcc phases cause the effect of constraint to elevated local tensile stresses to trigger the appearance of a brittle(e.g. cleavage) fracture mode. Such behavior has been found in testing of in-situ processed $Nb_5Si_3$/Nb composites[3-8] as well as laminates[9]. The intent of this work was to evaluate the mechanical behavior of Nb in $Nb_5Si_3$/Nb/$Nb_5Si_3$ laminates and to investigate some of the variables which could affect the degree of toughening in systems utilizing a "ductile" constituent based on a body centered cubic reinforcement. Systematic changes in interface strength were also performed in order to evaluate their effects on the mechanical behavior of the "ductile" ligament and resulting toughness. Such information was useful in analyzing the fracture behavior of the *in situ* composites described in Section III.

## Laminates Production and Toughness Testing

Two types of interface conditions were utilized in the laminates processed at CWRU, while the thickness of the ductile/tough Nb layer was also varied in a systematic manner. Interface conditions were varied by utilizing either diffusion bonding at high temperature and pressure or via low temperature bonding via the use of a structural adhesive. The thickness of the ductile/tough Nb layer was either 25 μm or 250 μm. For the laminates,

monolithic $Nb_5Si_3$ was prepared via mechanical alloying as described in our previous anuual reports. The $Nb_5Si_3$ powders were subsequently hot pressed into 2 in. diameter discs at 55 MPa at 1600 to 1700°C for 1-2 hrs. and subsequently electrodischarge machined and laminated with pure Nb foils (grain size 10μm) from Aldrich Chemical Company. The foils were either 25 μm or 250 μm thick. Figure 1 shows the schematic of diffusion bonding and the bend and notched specimens that were produced. Diffusion bonding was accomplished by pressing the laminate with 10 MPa pressure at 1473K for 5 hours. These variables were selected to limit the extent of Si diffusing into Nb, yet maintaining the strongly bonded interface. Additional laminates were produced using the structural adhesive EC 1386 from 3M incorporating either as-received Nb foil(Nb-AR) or vacuum heat treated Nb foil(Nb-VHT at 1473K/5 hr). Table I summarizes the materials and processing conditions, while Table II summarizes the microstructures and impurity contents resulting from the various processing schemes. The VHT condition was modeled to produce grain sizes similar to those found in the Nb(ss) samples. Testing for all laminates was conducted at both 298K and 77K.

The conclusions reached from the testing and analyses are summarized below, followed by an analysis of the results:

1. Thermal history, contamination, imposed constraint, and test temperature have a significant effect on the mechanical properties of the Nb(bcc) reinforcement as demonstrated by the smooth tension testing of Nb foils as well as model $Nb_5Si_3/Nb$ laminates.

2. Strong interface bonding produced a mixed cleavage/ductile fracture mode for the laminated samples tested at 298K with 100% cleavage exhibited at 77K. Quantitative fractography revealed that strong bonding generally produced cleavage fracture of Nb while debonded regions exhibited ductile fracture due to the relaxed constraint.

23

3. The effects of interface character on toughness was determined. Specimens with a strong interface(e.g. diffusion bonded) exhibited a higher toughness in comparison to epoxy bonded specimens when toughness was calculated using the peak load. This apparently arises due to the greater constraint required on the Nb ligament in the former case. However, the total energy(total area under the curve) was greater in the case of the epoxy bonded specimen which exhibited ductile rupture and significant energy absorbtion past peak load.

4. The layer thickness of the ductile/tough Nb exerted a strong effect on the fracture mode and toughness of the laminate. All diffusion bonded specimens exhibited a predominance of cleavage fracture of the Nb at 298K and 77K, whether the Nb was 25 $\mu$m or 250 $\mu$m thick. Despite the appearance of 100% cleavage fracture of the Nb, the toughness of the laminate was enhanced over that in the silicide. All adhesively bonded specimens tested at 298 K exhibited ductile rupture of the Nb, while testing at 77K produced cleavage fracture in laminates containing the 250 $\mu$m VHT Nb foil while 100% ductile rupture was exhibited by the laminates containing 25 $\mu$m VHT Nb foil. All adhesively bonded specimens containing AR Nb foil exhibited 100% ductile rupture under all conditions.

As shown in Table III, recrystallization and grain growth in the Nb-VHT produced a significant drop in yield strength from the 10 $\mu$m grain size Nb-AR. The increase in strength at both 298K and 77K in the Nb(ss) compared to the Nb-VHT with equivalent grain size is due to the presence of Si and O, both potent hardeners of Nb.

The fracture modes of two(i.e. Nb-VHT, Nb(ss)) of the three smooth tensile specimens of the 250 $\mu$m Nb foils were strikingly different from the third tested at 77K, as shown in Figures 2a-c. The Nb-VHT and Nb(ss) exhibited cleavage fracture at 77K, Figures 2b and 2c, while the Nb-AR exhibited ductile rupture. The change in fracture mode with decreasing temperature is consistent with the fracture of bcc materials[10-11] and

Orowan's proposal of brittle fracture stress[12]. Notching of pure Nb[13] and Nb(ss)[13, 14] has shown that while low temperature and constraint(i.e. notching promotes brittle fracture of both Nb and Nb(ss)), the concept[11,12] of a temperature-independent cleavage fracture stress appears to be obeyed over a range of temperatures. The experiments summarized in Section II confirm such behavior for both pure Nb and a range of Nb alloys tested at CWRU.

The large difference in fracture mode between the ductile rupture exhibited at 77K by the Nb-AR and the cleavage fracture exhibited by both the Nb-VHT and Nb(ss) may be due to the dependence of the cleavage fracture stress on grain size[11,15-19], the beneficial substructure retained in the rolled Nb-AR foil[20, 21] or strain aging effects which may enable mobile species such as C,N or O to pin dislocations during cooling from high temperatures. In general, large grained bcc metals exhibit a lower cleavage fracture stress in comparison to nominally identical fine grained specimens, while the epoxy bonded laminated specimens exposed to 450K for 1 hour failed to show any evidence of embrittlement at 298K limiting the relevance of the strain aging argument. Work [13,22] summarized in Section III illustrates the mechanisms primarily responsible for the changes in the fracture behavior of the above Nb ligaments.

Comparison of the constrained Nb behavior in Table IV to that of the unconstrained Nb in Table III reveals significant differences in fracture behavior and ductility of the Nb as well as strength. In the Nb(ss), the UTS is elevated via constraint while the ductility decreased due to the lamination. The fracture mode is similarly changed from ductile(i.e. unconstrained) to mixed cleavage and ductile(i.e. constrained). The ductile areas corresponded to areas of relaxed constraint due to multiple microcracking of the silicide as shown in Figure 3.

When these samples were tested at 77K, again the UTS was elevated in the Nb(ss) with a greater reduction in area than the Nb(ss) unconstrained(i.e. 8% vs 4%). No extensive

debonding or microcracking was observed correlating in part to the 100% cleavage fracture of the Nb.

The epoxy bonded DEN specimens exhibited flow stress, ductility, and fracture behavior very similar to that of the smooth Nb-AR and smooth Nb-VHT specimens. The in-situ SEM fracture experiments, as shown in Figures 4 and 5 revealed significant debonding of the Nb from the epoxy thereby relaxing the constraint and producing values for yield stress, UTS, and ductility nearly identical to the smooth specimens. Similar results were obtained for the laminates containing the 25 μm thick and the 250 μm thick Nb foils.

The average fracture toughness value of 8.6 MPa√m for diffusion bonded laminates tested at 298K represents a five fold increase as compared to that of the monolithic $Nb_5Si_3$(i.e. 1.7 MPa√m[9]). The significant toughness increase results from the energy absorbing capabilities of the Nb ligament and its ability to blunt propagating cracks in $Nb_5Si_3$. The SEN bend laminate tested at 298K exhibited a dual fracture mode as shown in Figure 6, with approximately 50% cleavage and 50% ductile fracture present through the specimen thickness. The SEN samples tested at 77K exhibited 100% cleavage fracture. The source(s) of this difference in fracture mode are due to the joint action of constraint and temperature-induced changes in the flow stress, enabling the brittle fracture stress of Nb to be exceeded at 77K. Little microcracking or loss of constraint accompanied the 100% brittle fracture of the Nb(ss) reinforcement in this case. Diffusion bonded laminates containing the 25 μm Nb ligaments failed by 100 % cleavage fracture at both 298 K and 77 K.

Consistent with our previous work summarized in previous AFOSR Annual Reports, the above data suggests that the mere appearance of cleavage failure is not necessarily detrimental to the toughness of such systems, provided a large amount of energy is absorbed during cleavage fracture. It is well known that pearlitic steels fail by cleavage fracture at 298K yet exhibit valid plane strain fracture toughness in excess of 50 MPa√m[23,25]. Recent fracture toughness tests both on Nb and Nb(ss) produced toughnesses in excess of 25MPa√m at 77K[13,14,24] as summarized in Section IV. In

order to evaluate the effects of contamination and grain size on the energy absorbing qualities of the materials tested, the uniaxial stress-strain curves of the various ligaments were analyzed to determine the energy to maximum load as well as the total energy absorbed by the specimens at both 298K and 77K. Tests at 298K did not produce significantly higher values for toughness. Figure 7 summarizes the calculations and supports the contention that more energy may be absorbed in a material which exhibits cleavage at 77K(i.e. Nb(ss)) than in a material which exhibits 100% ductile rupture(i.e. Nb-AR). Thus, the point may be concluded that one method of insuring tough composites is to have tough ligaments. "Ductility" is not necessarily the only important condition.

The adhesively bonded laminates incorporating the Nb-AR tested at 298K exhibited an average fracture toughness(i.e. from peak load) of 7.1 MPa$\sqrt{m}$, while epoxy bonded laminates incorporating Nb-VHT exhibited the average fracture toughness of 7.8 MPa$\sqrt{m}$. These values represent a decrease in the fracture toughness of 17% and 9% respectively, as compared to the diffusion bonded laminates. The lack of constrained Nb flow in the epoxy bonded specimens produces tensile data for the notched laminates which are nearly identical to the smooth tension specimens, thereby yielding lower toughness values than that obtained in the diffusion bonded specimens.

Further discussion is warranted on other measures of toughness for the tests conducted on the notched laminates of the type described presently. All of the toughness calculations shown in Table V utilized the peak load to determine $K_q$. A comparison of Figure(s) 8a & 8b to Figure(s) 9a & 9b reveals that while the toughnesses ($K_q$) calculated using the peak loads are not extremely different(e.g. 8.6MPa$\sqrt{m}$, 6.2 MPa$\sqrt{m}$, 7.1 MPa$\sqrt{m}$, and 7.8 MPa$\sqrt{m}$, respectively), the additional area past peak load is very different for the four conditions tested. The specimens exhibiting ductile rupture (i.e. epoxy bonded specimens in Figures 9a and 9b) clearly exhibit a greater amount of total energy absorbed when measured in this manner, in comparison to the diffusion bonded specimens (i.e. Figure 8a and 8b) which exhibited either 100% cleavage or a mixture of cleavage and ductile

27

fracture (i.e. Figure 6). Distinguishing between toughnesses calculated by using "peak load" and "total energy absorbed" is thus relevant in completely characterizing the toughness of such systems, as pointed out elsewhere[26]. Similar conclusions are reached when comparing the results obtained for the laminates containing the 25 $\mu$m Nb foil, although the magnitude of toughening is less because of the thinner Nb ligament.

# Laminate Processing and Properties References

1. P. A. Mataga, B.J.Dalgleish, R.M. McMeeking and A.G. Evans, *Acta Metall.*, **36**, 945, (1988).
2. M. F. Ashby, F.J Blunt and M. Bannister, *Acta Metall.*, **37**, 1847, (1989).
3. J.D.Rigney, J.J. Lewandowski in M.D. Sacks(ed.),*Proce. 2nd. Int. Ceramic Science and Technology Congr.-Advanced Composite Materials*, American Ceramics Society, Westerville, OH, 519, (1990).
4. M.G. Mendiratta, J.J. Lewandowski and D.M. Dimiduk,*Metall. Trans. A*, **22**, 1573, (1991).
5. J.D.Rigney, P. Singh, and J.J. Lewandowski, *Journal of the Mineral, Metals & Materials Society*, **44**, 36, (1992)
6. J.D.Rigney, J.J.Lewandowski,L.Matson, M.G.Mendiratta, D.M.Dimiduk,*Mater. Res. Soc. Symp. Proc.*, MRS, **213**, 1001, (1991).
7. J.J. Lewandowski, D.M. Dimiduk, W. Kerr and M.G. Mendiratta,*Mater. Res. Soc. Symp. Proc.*, **120**, 103, (1988).
8. M.G. Mendiratta and D.M. Dimiduk,*Metall. Trans. A*, **24A**, 501 (1993).
9. J. Kajuch, J.D. Rigney and J.J. Lewandowski,*Mater. Sci. Eng.*, **A115**, 59, (1992).
10. G.E. Dieter,*Mechanical Metallurgy*, 3rd ed., McGraw-Hill, (1986).
11. J.F. Knott,*Fundamentals of Fracture Mechanics*, Butterworths, London, (1973).
12. E. Orowan,*Trans. Inst. Engrs. Shipbuilders Scot.*, **89**, 165, (1945).
13. J.D. Rigney and J.J. Lewandowski, *Metall Trans. A*, in press,(1996).
14. M.G. Mendiratta, R. Goetz, D.M. Dimiduk and J.J. Lewandowski,*Metall. Trans. A*, **26A**, 1767 (1993).
15. M.A. Adams, A.C. Roberts, R.E. Smallman,*Acta Metall.*, **8**, 328, (1960).
16. A.A. Johnson,*Acta Metall.*, **8**, 737, (1960).
17. J.D. Embury in H. McQueen(ed.),*Strength of Metals and Alloys*, Proc. ICSMA, (1985).
18. A.W. Thompson and J.F. Knott,*Metall. Trans. A*, **24A**, 523, (1993).
19. R.O. Ritchie, J.F. Knott, and J.R. Rice,*J. Mech. Phys. Solids*, **21**, 395, (1973).
20. A. Ball, F.P. Bullen, F. Henderson, H.L. Wain in P.L. Pratt(ed.),*Fracture 1969*, Chapman and Hall, London, 327, (1969).
21. M.F. Ashby and J.D. Embury,*Scripta Metall.*, **19**, 951, (1985).
22. A. Samant, J.D. Rigney and J.J. Lewandowski, *Metall. Trans. A* , in review (1996).
23. D.J. Alexander and I.M. Bernstein,*Metall. Trans. A*, **20A**, 2321, (1989).
24. J.D. Rigney,*Ph.D Thesis*, Case Western Reserve University, Cleveland, Ohio,(1993).
25. J.J. Lewandowski in M. Singh(ed),*In-Situ Composites*, TMS, Warrendale, PA, 159, (1994).
26. L. Xiao and R. Abbaschian, *Metall. Trans. A*, **24A**, 403, (1993).

| Nb foils (250 µm) | Condition |
|---|---|
| 1. Nb-AR | As Received |
| 2. Nb-VHT | 1473 K/5 hr vacuum treatment |
| 3. Nb(ss) | Nb foil diffusion bonded to $Nb_5Si_3$ 1473 K/5 hr and removed |
| | |
| $Nb_5Si_3$/Nb/$Nb_5Si_3$ Laminates | Condition |
| 1. $Nb_5Si_3$/Nb(ss)/$Nb_5Si_3$ | 1473 K/5 hr @ 10MPa - Diffusion Bonded |
| 2. $Nb_5Si_3$/E/Nb-AR/E/$Nb_5Si_3$ E = Epoxy | 450 K/1 hr @ 0.16 MPa - Epoxy Bonded |
| 3.$Nb_5Si_3$/E/Nb-VHT/E/$Nb_5Si_3$ E = Epoxy | 450 K/1 hr @ 0.16 MPa - Epoxy Bonded |

Table I Materials and Processing Conditions

| Nb Foils | Grain Size (µm) | C (ppm) | O (ppm) | N (ppm) | H (ppm) | Si (ppm) |
|---|---|---|---|---|---|---|
| AR 250µm | 10 | <10 | <125 | <50 | <5 | <100 |
| VHT 250µm | 210 | 420 | 490 | 120 | NA | 90 |
| Nb(ss)250µm | 210 | 210 | 1300 | 190 | NA | 1050 |
| $Nb_5Si_3$ | 10 | 980 | 1260 | NA | NA | 16.9wt% |
| AR 25µm | 10 | | | | | |
| VHT 25µm | 50 | | | | | |

Table II Microstructrual Analyses and Impurity Content of Nb Foil and $Nb_5Si_3$ Matrix

| MATERIAL & CONDITION | TEST TEMP. (K) | $\sigma_y$ (MPa) | UTS (MPa) | AREA REDUCTION (%) | FRACTURE MODE |
|---|---|---|---|---|---|
| Nb-AR | 298 | 268 | 358 | 78 | Ductile Rupture |
| Nb-VHT | 298 | 186 | 222 | 79 | Ductile Rupture |
| Nb(ss) | 298 | 363 | 390 | 76 | Ductile Rupture |
| | | | | | |
| Nb-AR | 77 | 730 | 900 | 93 | Ductile Rupture |
| Nb-VHT | 77 | 661 | 765 | 6 | Cleavage |
| Nb(ss) | 77 | 844 | 960 | 8 | Cleavage |

Table III Tensile Properties of Nb Reinforcement in Various Conditions

| SAMPLE NUMBER | DISTANCE OF NOTCH FROM $Nb_5Si_3$/Nb INTERFACE | TEST TEMP. (K) | BEND BAR DIMENSIONS (mm) | $P_{qmax}$ (kg) | $K_q$ (MPa$\sqrt{m}$) |
|---|---|---|---|---|---|
| 1 | 112 μm | 298 | 8x4x40 | 20.8 | 7.1 |
| 2 | 240 μm | 298 | 8x4x40 | 28.3 | 8.9 |
| 3 | 145 μm | 298 | 8x4x40 | 23.1 | 7.4 |
| 4 | 20 μm | 298 | 8x4x20 | 46.2 | 8.4 |
| 5 | 20 μm | 298 | 8x4x20 | 59.1 | 11.4 |
| 6 | 275 μm | 77 | 8x4x46 | 15.7 | 6.2 |

Table V $K_q$ Toughness Values of Diffusion Bonded Laminates tested in 3-point Bend

Nb5Si3
Nb
Nb5Si3

4 mm
0.25 mm
4 mm

Pressure : 10 MPa
Temperature: 1200 °C
Time : 5 hours

8 mm
4 mm

3.88 mm
P

5.96 mm
2.5 mm
7.20 mm

3.71 mm
7.97 mm
P

Figure 1 Schematic of diffusion bonded laminate production.

Figure 2 Nb unconstrained tensile fracture surfaces at 77K
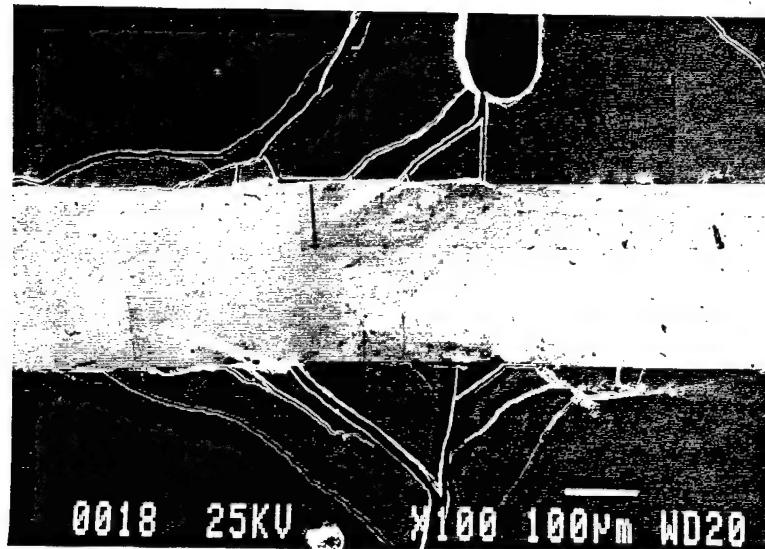a) Nb-AR b) Nb-VHT c) Nb(ss).

Figure 3 Multiple cracking of silicide in a diffusion bonded laminate tested in three point bending at 298K. Ductile fracture predominates in such regions of multiple microcracking.
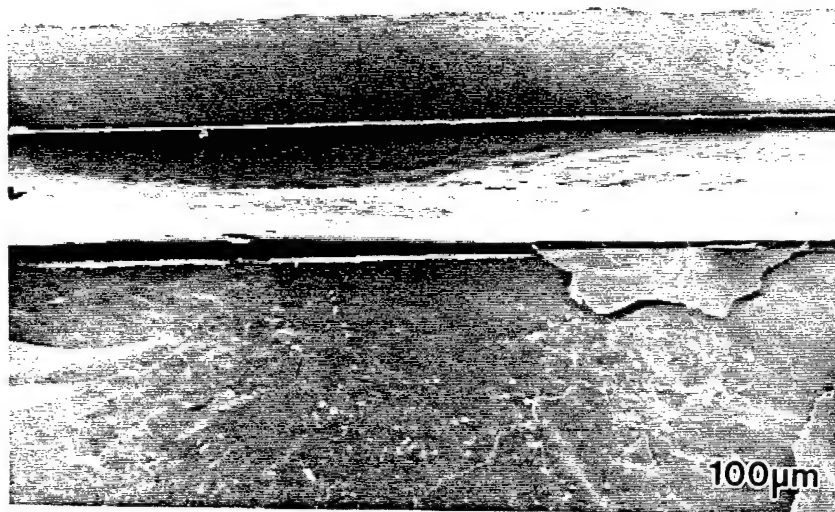


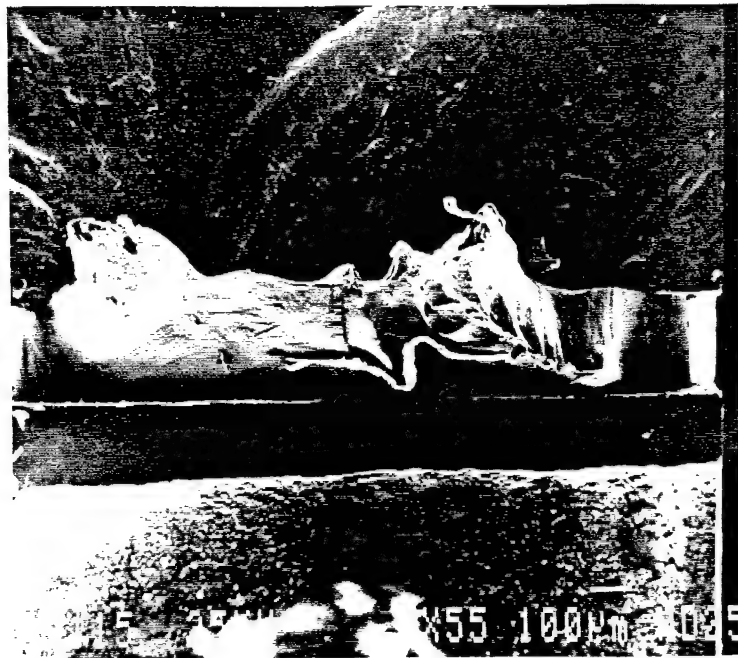Figure 4 Ductile rupture present in Nb-AR DEN laminates. In situ view from deformation stage.

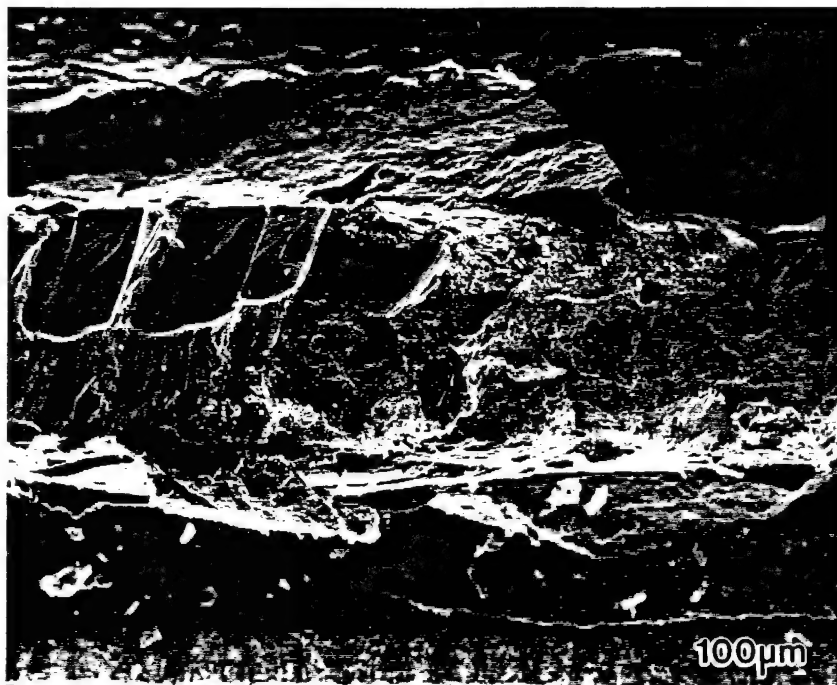Figure 5 Ductile rupture present in Nb-VHT DEN laminates. In situ view from deformation stage.



Figure 6. Fracture surface of Nb ligament in diffusion bonded laminate tested in three point bending at 298K.
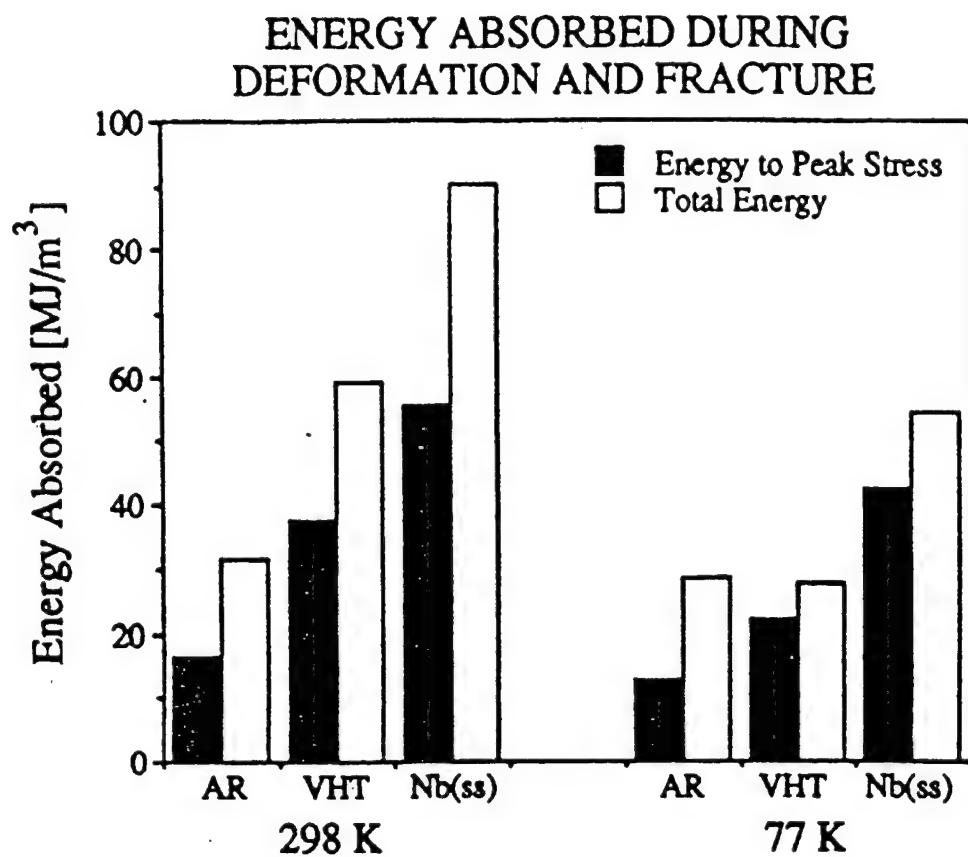
37

Figure 7  Comparison of Energy Absorbed during deformation and fracture at 298K and 77K.
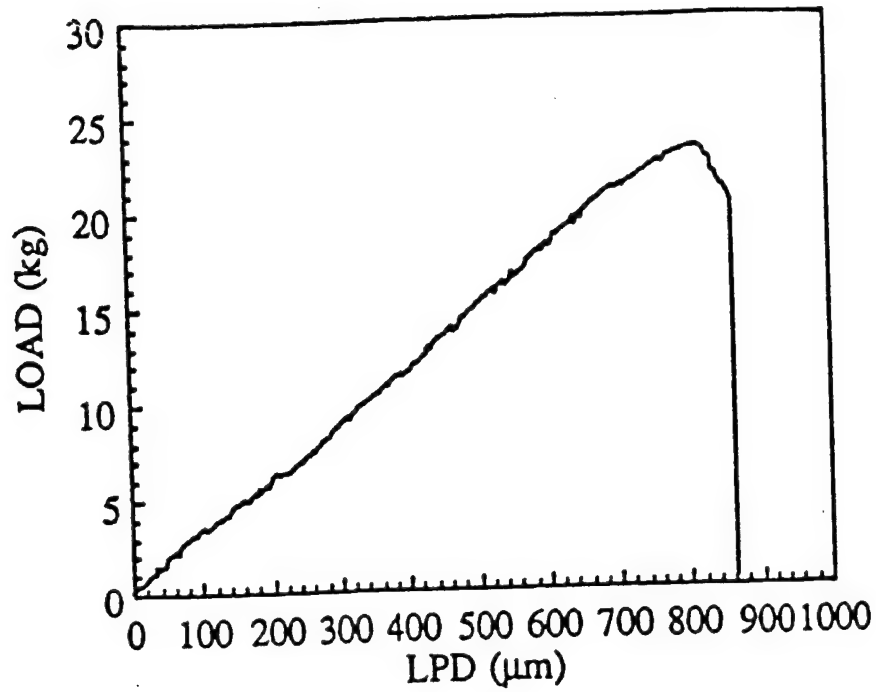
Figure 8a Load-load point displacement trace of a diffusion bonded laminate sample
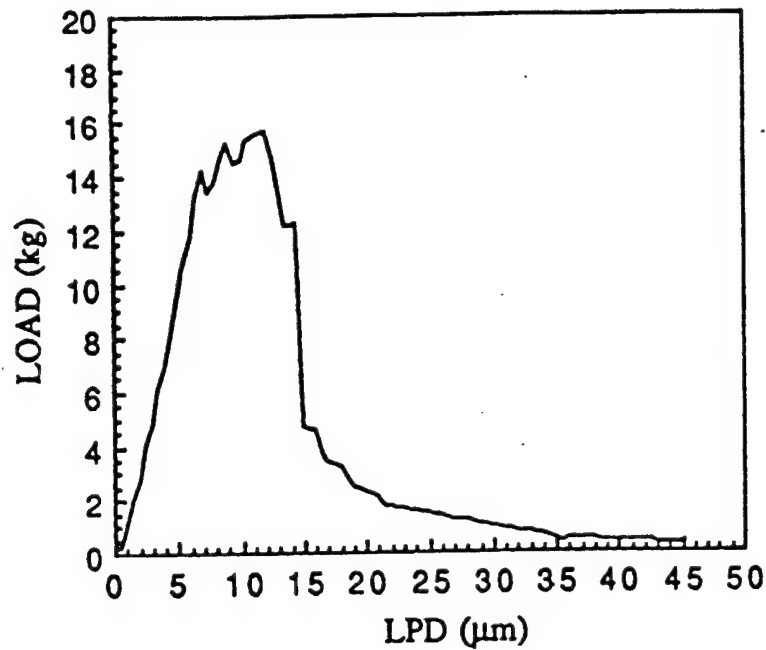tested in three point bending at RT(298K)[15].



Figure 8b Load-load point displacement trace of a diffusion bonded laminated sample
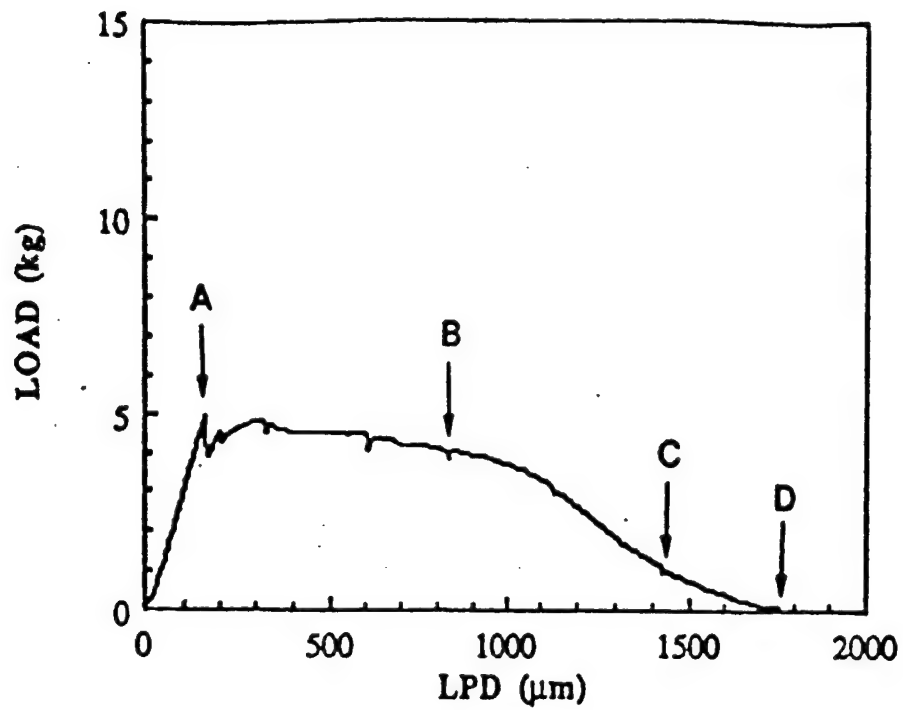tested in three point bending at liquid nitrogen temperature(77K).

Figure 9a Load-Load Point Displacement Trace of structural adhesive bonded laminate with Nb-AR reinforcement tested in three point bending at RT(298K).
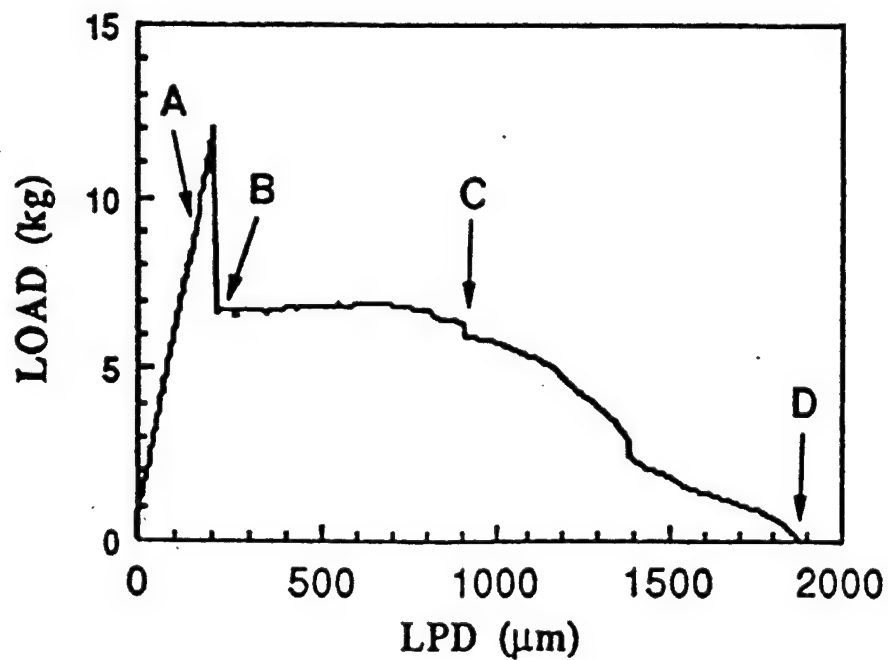


Figure 9b Load-Load Point Displacement Trace of structural adhesive bonded laminate with Nb-VHT reinforcement tested in three point bending at RT(298K).

40

# III - Mechanical Behavior of In-Situ Nb5Si3/Nb Composites

In addition to the studies being conducted on the laminated systems described earlier, a significant research effort has been focused on understanding the fracture toughness of in-situ composites based on the Nb-Si system and prepared at Wright Patterson Air Force Base. This work has been conducted in close collaboration with researchers at UES, Inc. as well as with researchers at WPAFB. As such, some of the papers arising from this work are co-authored with Drs. M. Mendiratta and D. Dimiduk. More recent work has also begun to investigate the mechanical behavior of DS eutectics prepared by General Electric at their Schenectady Research Laboratory.

The microstructure of the cast/extruded composite is shown in Figure 1. Significant previous work has documented the effects of subsequent working and heat treatment on the properties (1-3). The fracture toughness of extruded and heat treated Nb-10 at% Si as well as Nb-15 at% Si specimens have been determined using bend bar fracture toughness specimens tested inside of a scanning electron microscope in order to view and document the evolution of the "bridged zones" as well as determine the resistance-curve of the in-situ composites. In order to calculate and analyze the R-curve in such systems, it is essential to know the instantaneous crack length. The in-situ SEM deformation stage provides such information with the additional capability of video recording the deformation and fracture events occurring at the crack tip. These experiments have been summarized in our various previous AFOSR Annual Reports.

Of particular interest in recent years were the effects of changes in loading rate and test temperature on the fracture toughness as these will have important practical applications. In order to more fully investigate the effects of loading rate on fracture toughness of such systems, a series of experiments were conducted on identical in-situ composites where the loading rate was varied over five orders of magnitude and the resulting toughness

41

determined. In addition, identical experiments were conducted at 77K in an attempt to induce cleavage fracture of the Nb and to determine the effects of such behavior on the toughness(4). Figure 2 summarizes the effects of changes in loading rate and test temperature on the fracture toughness. It is shown that the toughness is negligibly affected for the conditions tested, despite the fact that the fracture morphologies at both high loading rates and low temperatures are predominantly cleavage fracture as shown in the quantified fracture surfaces summarized in Figure 3. It is clear from this work as well as that presented in the previous section for the laminates tested at 77K that the mere appearance of cleavage fracture does not necessarily accompany low toughness. It is possible that significant amounts of energy can be absorbed during cleavage fracture, producing a fracture appearance that appears macroscopically brittle yet exhibits (relatively) high toughness as shown in Figure 2. This assertion is further corroborated by the fracture toughness results for the pure Nb and Nb alloys tested at 77K, summarized in Section IV.

# References for Mechanical Behavior of Composites

1.  J.J. Lewandowski, D. Dimiduk, W. Kerr, and M.G. Mendiratta, *Mater. Res. Soc. Symp. Proc.* **120**, 103, (1988).
2.  M.G. Mendiratta, J.J. Lewandowski, and D.M. Dimiduk, *Metall. Trans. A.,* **22**, 1573, (1991).
3.  M.G. Mendiratta and D.M. Dimiduk, *Mater. Res Soc. Symp. Proc.,* **133**, 441, (1989).
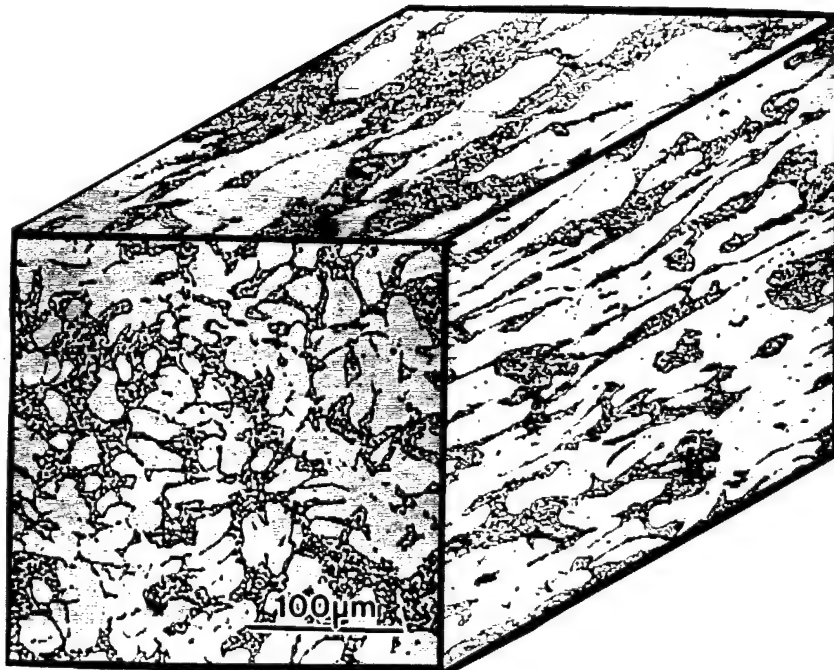4.  J.D. Rigney and J.J. Lewandowsk, *Metall. Trans. A,* in press, (1996).

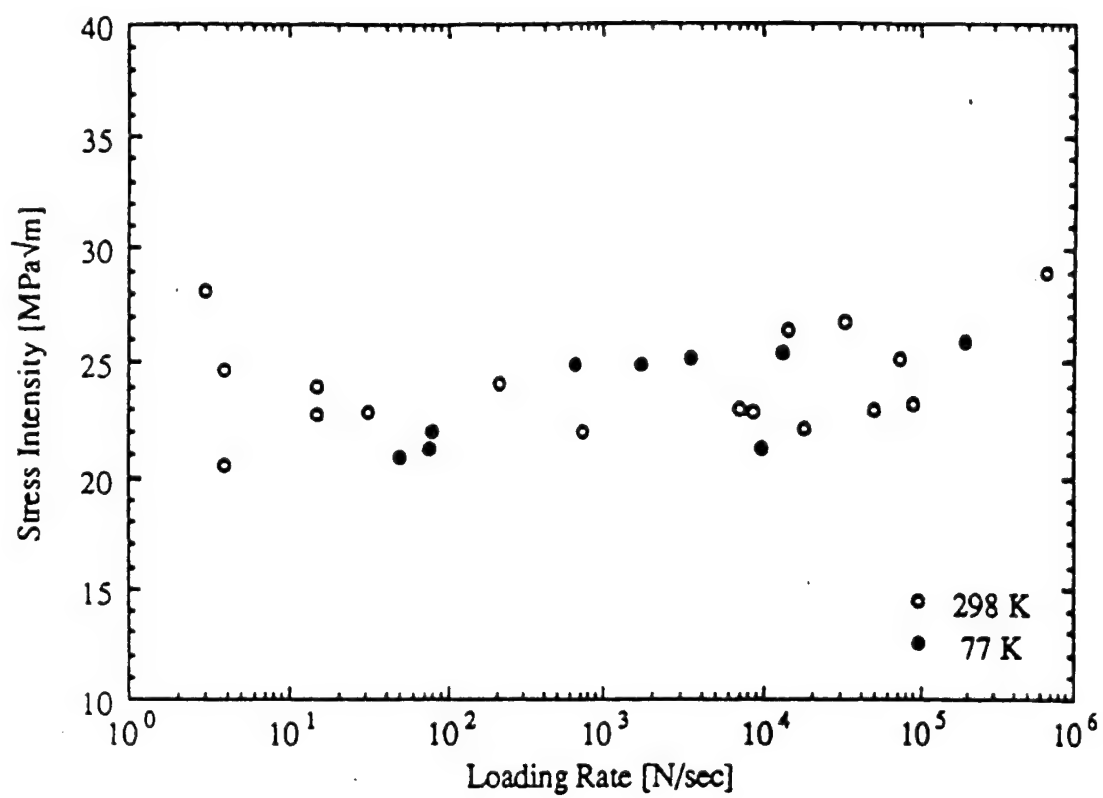Figure 1. Microstructure of cast/extruded Nb-15 at% Si.

Figure 2. Fracture toughness as a function of loading rate at both 298K and 77K. No effect of lowering the test temperature on the measured toughness was observed at any rate.
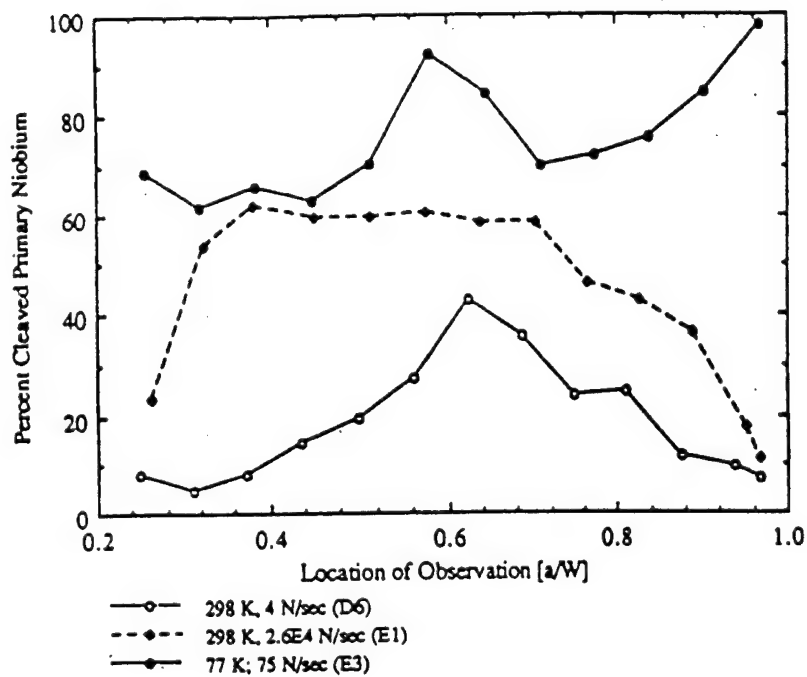
Figure 3. Temperature and crack tip positions effects on the fracture behaviors of the $Nb_p$. The low temperature sample was loaded at a rate(75 N sec$^{-1}$) slightly greater than that used to fracture the 298K sample(4 N sec$^{-1}$) of the lowest curve.

# IV - Fracture Toughness and Cleavage Stress of Nb and Nb Alloys

*(1) Effect of Grain Size, Test Temperature, Alloy Composition on Cleavage Fracture Stress and Toughness of Nb and Nb alloys.*

Throughout the work conducted at CWRU and that summarized in the previous pages, it is clear that the constraint/lamination of brittle matrices to Nb may elevate stresses to a level that is sufficient to induce cleavage fracture of the nominally ductile Nb. As such, it is essential that the stresses required to produce cleavage fracture of Nb and Nb alloys be determined with some certainty in order to enable predictive models to be developed. In particular, the effects of systematic changes in grain size, test temperature, and alloy content on the cleavage fracture stress and fracture toughness were determined, using the information developed under a previous AFOSR grant to guide the selection of relevant grain sizes and other variables.

In particular, the concept of a temperature-independent cleavage fracture stress proposed by Orowan (1) has been explored for Nb and Nb alloys. Blunt notched bend bars (2,4,11) shown in Figure 1 have been tested over a range of test temperatures in order to determine the effects of systematic changes in grain size and alloy composition on the magnitude of the cleavage fracture stress. Such experiments are extensively utilized in the ferrous metallurgy community (2) and one of the P.I.'s has extensive experience in the use of such specimens (3-5) that are combined with existing finite element analyses (4,5) in order to determine the local stresses required to initiate and propagate cleavage fracture. Although extensive information exists on the conditions/microstructures controlling cleavage fracture in ferrous based systems, little information of this nature exists for Nb and Nb alloys. In particular, the effects of changes in grain size and solid solution additions of

47

either Si or Zr on the magnitude of the cleavage fracture stress have been presently determined. Such information has direct relevance for the interpretation of the fracture behavior of the laminates and in-situ composites already discussed.

In addition to the cleavage fracture stress measurements, fracture toughness experiments have been conducted over a similar temperature range. Such information will again be useful in interpreting the effects of test temperature on the toughness of the laminates as well as the in-situ composites discussed earlier.

Fractography has been utilized in both the notched bend and fracture toughness experiments to determine the fracture initiation sites as well as to compare to existing models for fracture toughness of bcc systems (6).

*(2) Experimental Methods*

*Materials Tested:*
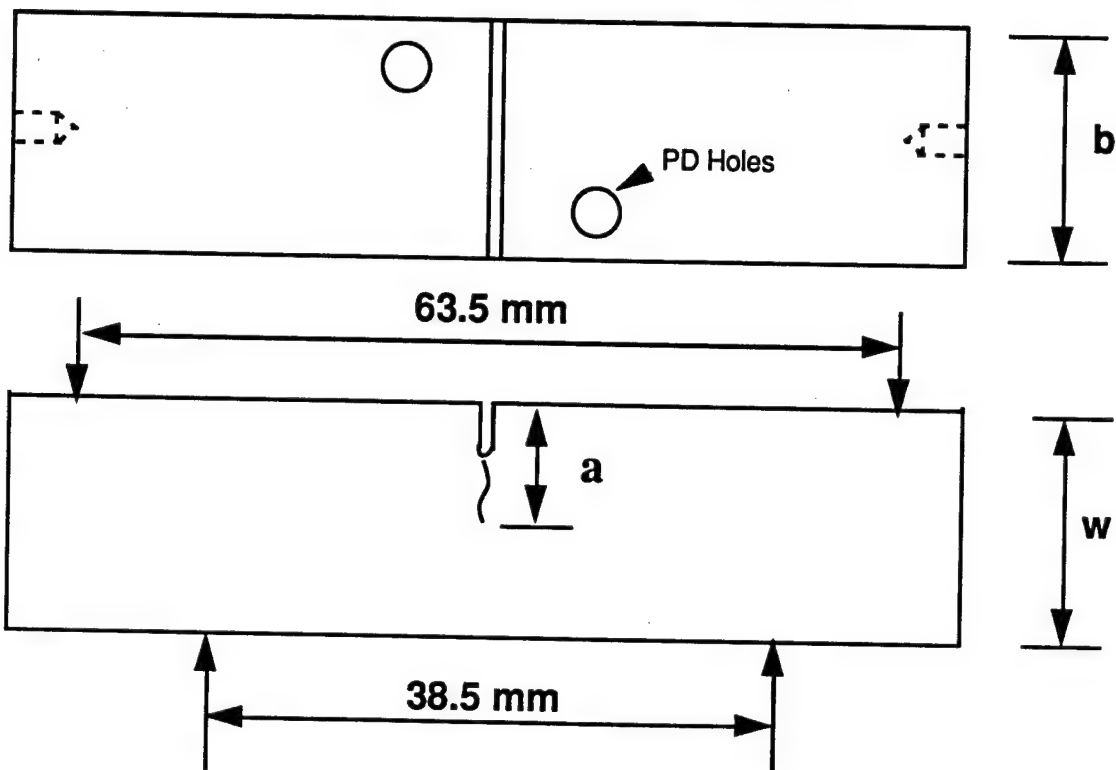
The two different materials tested were commercially pure niobium (henceforth referred to as Nbp or Nbpure) and a solid solution alloy of niobium with 1 wt. % zirconium (henceforth referred to as Nb - (ss) Zr). The materials, obtained from Cabot Corporation, Bethlehem, PA, were supplied in 12.7 mm thick X 150 mm X 150 mm square plates, in the as-rolled, unannealed condition. Table 1 lists the chemistry of the as-received materials as reported in the wet chemical analysis performed by Herron Testing Laboratories, Cleveland, OH [7].

*Grain Growth Studies and Heat Treatments:*

Grain growth studies were conducted on the as-received materials to obtain the desired average grain sizes, to be reproduced in the actual samples to be tested. Approximately 0.25 inch (6.35 mm) cuboid coupons of both materials were heat treated for either one hour or two hours in a Lindberg Hevi-Duty (Model 59545) Alumina/Mullite tube furnace. The coupons were wrapped in 0.006 inch or 0.007 inch (0.1524 mm or 0.1778

mm) tantalum foil and the heat treatments were carried out under a constant flow of Ultra-High Purity argon gas. Care was taken to place the coupons in the center of the hot zone of the furnace. After the heat treatment and overnight cooling in the furnace, the coupons were sectioned in three mutually perpendicular directions to observe the grain texture in all possible directions. After mounting in bakelite, these were ground using SiC grinding papers from grit sizes 180 thru 4000. After this the samples were left overnight in a Buehler Vibromet I polisher with a 0.05 micron alumina powder suspension to obtain a micropolish. These samples were then etched using a solution of 60 vol.% lactic acid, 20 vol.% nitric acid and 20 vol.% hydrofluoric acid for 40 seconds. 100X pictures of these etched surfaces were taken using a Nikon Microphot-FX optical microscope. Average grain sizes were calculated by an approximate linear intercept method from 3-5 pictures. About 2-3 time-temperature combination heat treatments were done to ensure grain size reproducibility. Fig. 2 shows the results of the grain size study for the Nb and Nb-(ss)Zr alloys. After satisfactory grain sizes were obtained in the test coupons, the actual bend bars were heat treated. These bend bars were also wrapped in tantalum foils. Care was taken to locate the notch region of each bend bar at the same location in the furnace where the coupons were heat treated. These heat treatments were also carried out under an argon gas flow. After heat treatment, each bend bar was ground using a 120 micron diamond bonded abrasive wheel, taking off approximately 100 microns from the two width sides, to remove any oxide scales on layers.

# 4 POINT BEND TOUGHNESS SPECIMEN



# 4 POINT BEND CLEAVAGE
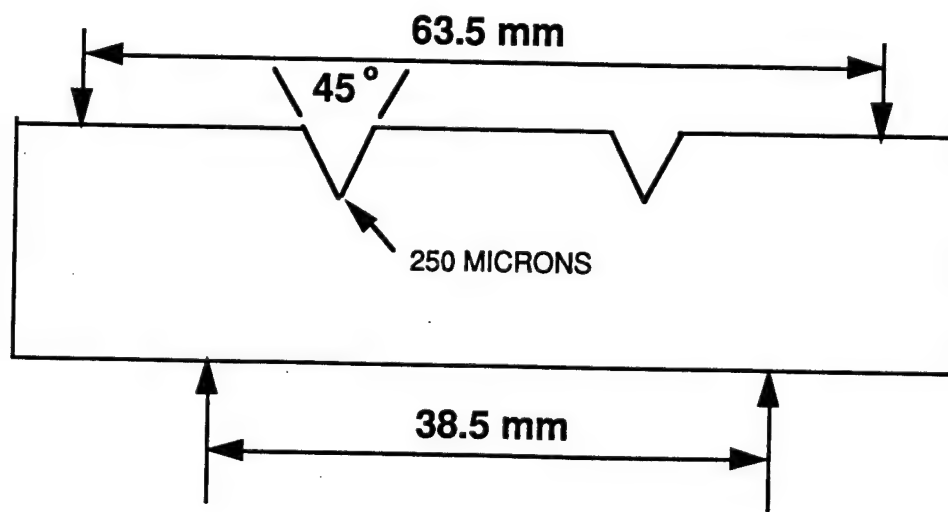# FRACTURE STRESS SPECIMEN



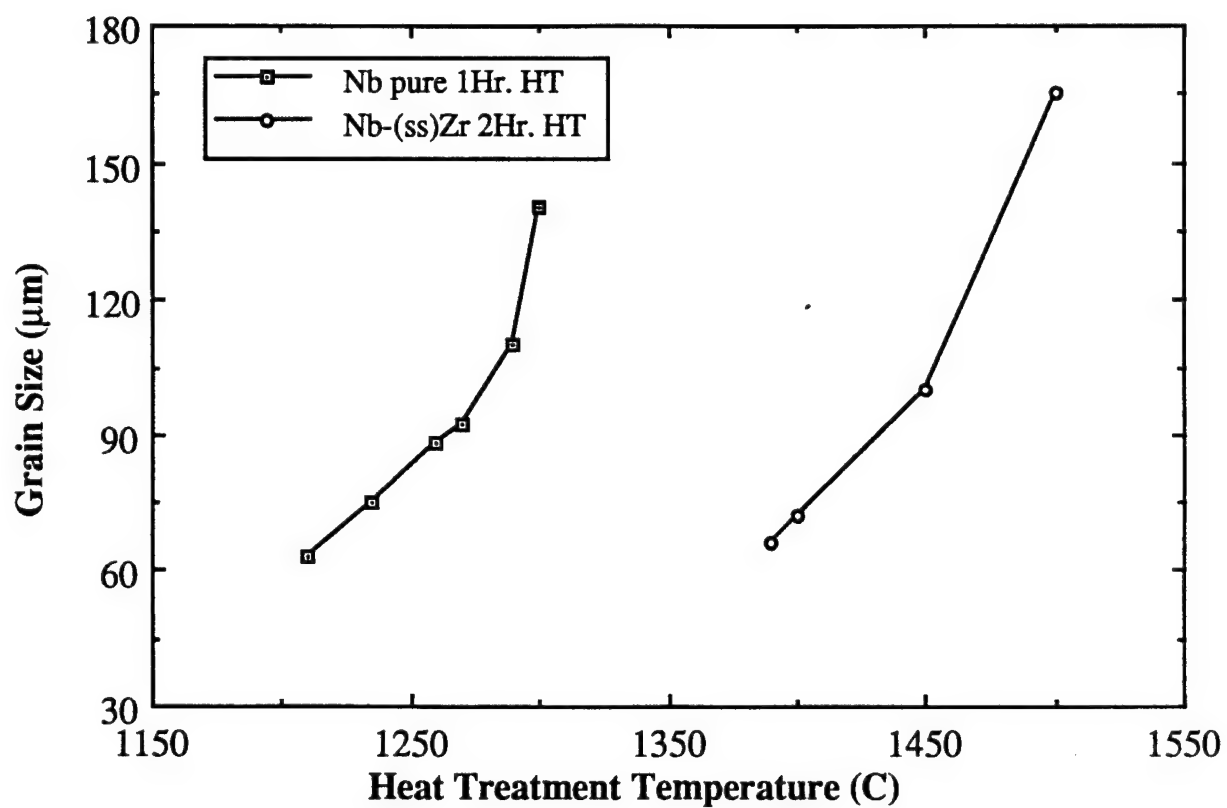Fig. 1  Schematic showing the two kinds of samples tested

Fig. 2 Grain size as a function of heat-treatment time and temperature.

| Material | Oxygen (ppm) | Nitrogen (ppm) | Silicon (at. %) | Zirconium (at. %) |
|----------|--------------|----------------|-----------------|-------------------|
| Nb pure | 205 | 50 | 0.03 | - |
| Nb - (ss) Zr | 90 | 188 | - | 0.61 |

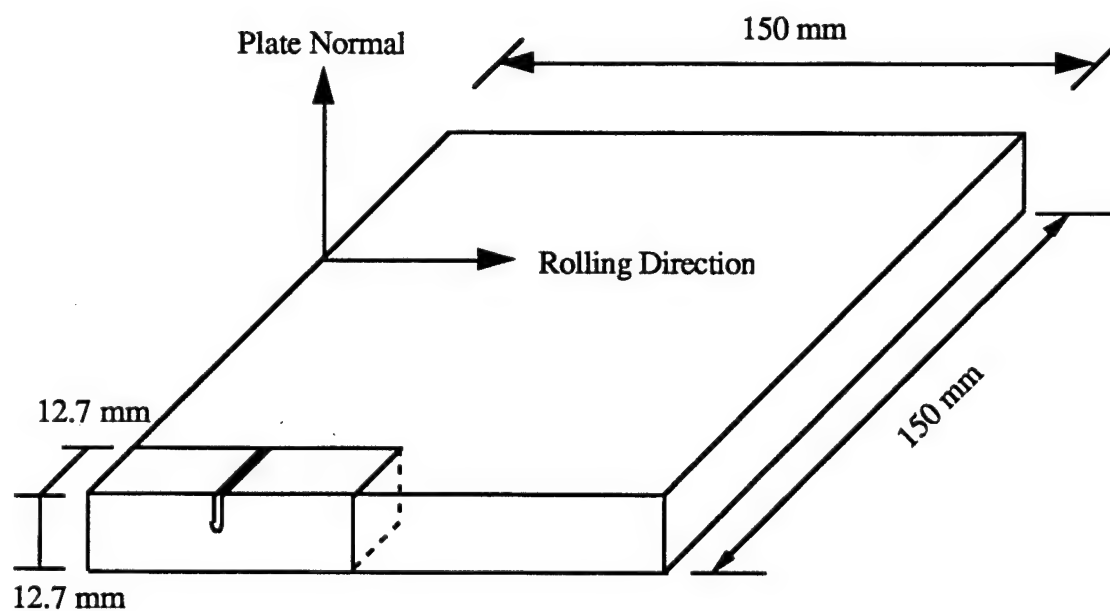Table I Chemistry of the as-received materials [4].



Fig. 3 Schematic of the orientation of the samples machined from the plates.

*Mechanical Testing:*

*Sample Preparation and Geometries:*

Bend bars were machined from the as-received Nbpure and Nb - (ss) Zr plates. The samples were oriented such that the longitudinal section of each was parallel to a rolling direction as indicated in Fig. 3. The bend bars tested were each 3 inches (76.2 mm) long with an approximately square cross section of 0.5 inch (12.7 mm) side. Fig. 1 is a schematic showing the two kinds of samples tested. The fracture toughness samples were starter notched in mid-span with a 300 micron diameter diamond wire on a model 3241 Well - Precision diamond saw upto an approximate depth of 0.4W (W = sample width). The two v-notches on the double notched cleavage fracture stress samples were symmetrically centered 20 mm apart and were about 4.25 mm deep with a flank angle of $45^\circ$ and a root radius of 250 microns. The loading spans used in the two different tests are indicated in Fig. 1.

*Fracture Toughness Testing:*

The samples were fatigue precracked in a three point bend configuration in accordance with ASTM E-399 standards [8]. The precracking was done at room temperature on a MTS servohydraulic machine using a MTS 442 controller and a Digital PDP-11 computer, at a frequency of 25 Hz and a stress ratio (R) of 0.1. Potential drop crack length measurement techniques were used to measure instantaneous crack lengths during precracking. A Sorensen SR 10-50 power supply was used to provide a constant 20 amp DC current input to the sample. The change in potential was measured across the notch as shown in Fig. 1. This signal was amplified using a Ectron series 750 differential DC amplifier. The amplified signal was fed to the PDP-11 computer to complete the feed-back control loop. The samples were precracked at moderate loads of about 500-600 lb. resulting in a stress intensity range (DK) of 8-10 MPa $\sqrt{m}$. It was impractical to precrack the samples at the temperature they were to be tested. On the other hand, it was also not possible to precrack the samples within the stress intensity range suggested by the ASTM

E-399 standard, because this stress intensity range was found to lie below the threshold $(K_{th})$ value for the materials under consideration. The samples were precracked to a final crack length between 0.45 W to 0.55 W as specified in the standard [8]. The precracked samples were tested in a four point bend configuration under displacement control at a load point displacement (LPD) rate of 0.6 mm/minute. The four point bend configuration was chosen because it is the closest simulation of a pure bending situation and minimizes the component of shear present in three point bending. Tests were done on a MTS servohydraulic machine with a MTS 458.20 MicroConsole controller. Load, load point displacement (LPD) and crack opening displacement (COD) were monitored during the tests, using Strawberry Tree Inc. Quicklog v3.1 data acquisition software. The lowest test temperatures were obtained by testing the samples directly immersed in liquid nitrogen. Higher temperatures were obtained by varying the flow of liquid nitrogen vapors around the samples. It was observed that even though it took longer to get to the desired temperature by this method, it was easier to hold the sample at this temperature during the test. Test temperature was measured using a $0^o$ C referenced Type K thermocouple mounted on the sample surface near the notch, and a Keithley 175 Autoranging multimeter. For each material-grain size combination, tests were done at three different temperatures. A low temperature (83 K - 90 K), an intermediate temperature (110 K - 130 K ) and a high temperature (135K-150K).

For samples that exhibited little or no plasticity before unstable crack propagation, a stress intensity factor was calculated at the peak load. This was then checked for validity in accordance with the standards [8]. For samples which exhibited appreciable crack tip blunting or other indications of stable crack growth, an initiation toughness was calculated at the first point of inflection in the load displacement trace. In both cases, the stress intensity factors were calculated according to the following equations [9].

$$K_I = \frac{3Pl}{bw^2}\sqrt{\Pi a}.F(\alpha), \alpha = \frac{a}{w} \qquad \qquad ......(1)$$

$$F(\alpha)=1.122-1.121\alpha+3.74\alpha^2+3.873\alpha^3-19.05\alpha^4+22.55\alpha^5 \qquad ......(2)$$

Where: P = Failure load (KN)

l = One-half the difference in the two spans used in the four point

bend test (cm)

b = Sample thickness (cm)

w = Sample width (cm)

a = Crack length after precracking (cm)

F(a) = Specimen geometry factor

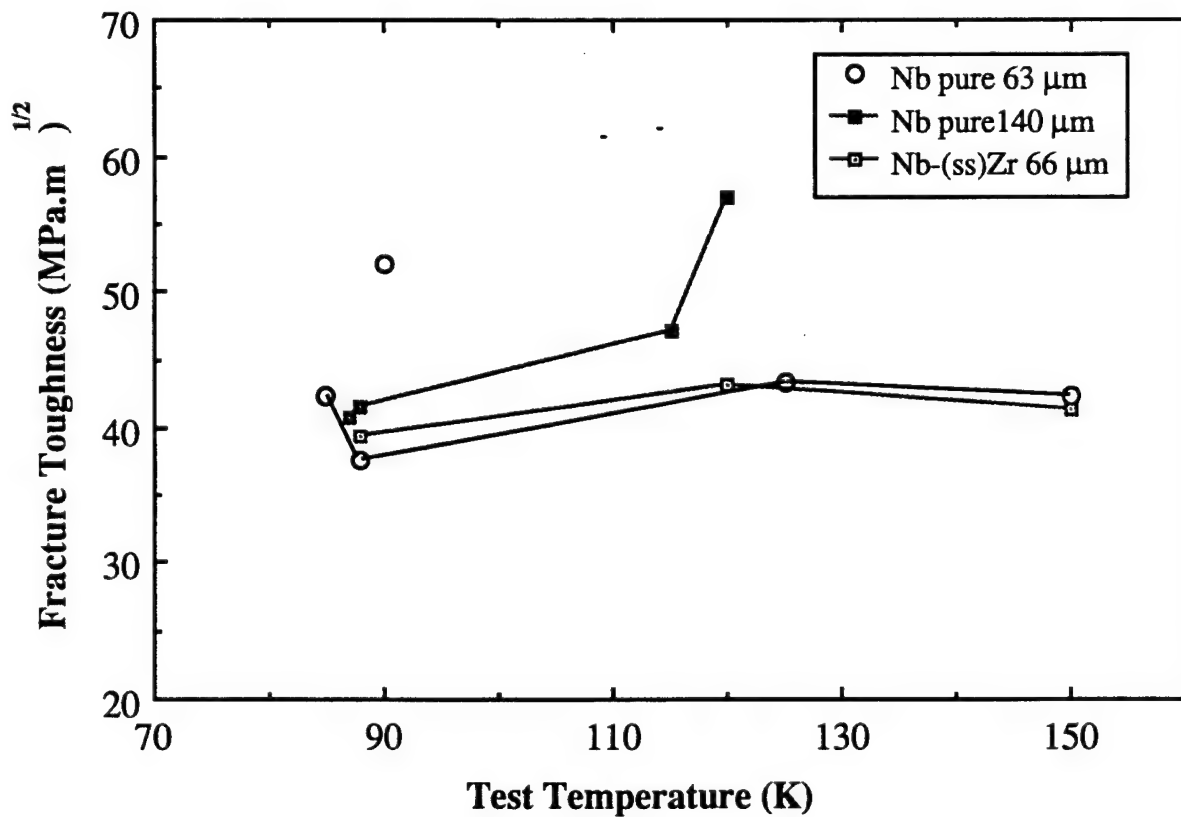$K_I$ = Stress intensity factor (MPa $\sqrt{m}$ )



Fig. 4 Fracture toughness as a function of test temperature.

Fig. 4 shows the preliminary results on the fracture toughness over a range of temperatures for both the pure Nb and Nb-(ss)Zr specimens. It is seen that the thoughness at 80K is still in excess of 40 MPa $\sqrt{m}$, and there is not a great dependance of peak toughness on the test temperatures over the range 80-150K. Additional work has focussed on fractographic observations of cleavage fracture initiation sites and has shown them often to exist at roughly the peak stress location in the precracked samples (11).

*Cleavage Fracture Stress Testing:*

The double notched bend bars used to determine the cleavage fracture stress are shown schematically in Fig. 1. These were tested in four point bend and were dimensionally similar to the single notched bend bars used by Griffiths and Owen for their elastic-plastic stress analysis for a notched bend bar in plane strain bending [10]. The 20 mm distance between the two notches ensures that the plastic zones ahead of them will not interfere with each other. The loading spans were so chosen that both the notches were located within the inner loading span during testing. Since both the notches will experience the same bending moment, and hence the same stress state, both should have the same propensity for fracture. However, one of the two notches will either be slightly deeper (due to machining limitations) or microstructurally more favorable for fracture. In this event, the notch that fractures can be used for fracture surface studies, while the other notch can be serially sectioned to locate and identify fracture initiation events.

Similar to the fracture toughness testing, three different temperature ranges were selected for each material-grain size combination. Load, load point displacement (LPD) and crack opening displacement (COD) on one of the two notches were monitored. Temperature was measured with a thermocouple mounted near the notch, and similar cooling media as before, were used. The four point bend testing was done on a MTS servohydraulic machine with a MTS 458.20 MicroConsole controller. Moderate load point displacement rates of 0.6 mm/minute were used.

The Griffiths and Owen finite element analysis [10] approximates the peak intensification of the principal tensile stress ahead of a blunt notch. A ratio of the nominal stress ($s_{nom}$) experienced by the bend bar, to the global yield strength ($\sigma_y$) of the material, is used to calculate this peak tensile stress. The nominal stress ($\sigma_{nom}$) can be calculated as follows:

$$\sigma_{nom} = \frac{6M}{b(w-a)^2} \qquad\qquad ......(3)$$

$$M = \frac{P}{4}(S_2 - S_1) \qquad\qquad ......(4)$$

Where: M = Bending moment experienced by the bar (N.m)

  b = Sample width (m)

  w = Sample width (m)

  a = Notch depth (m)

  P = Load to failure (N)

  $S_2$, $S_1$ = Outer and inner loading spans in the four point bend

configuration (m)

Fig. 5 is a plot of the ratio of the maximum principal tensile stress ($\sigma_{1max}$) to the yield strength ($\sigma_y$), as a function of the ratio of the nominal stress ($\sigma_{nom}$) to the yield strength ($\sigma_y$) [10]. The ratio of the nominal stress ($\sigma_{nom}$) calculated in equation (3) to the yield strength ($\sigma_y$) is then used with the graphical results in Fig. 5 to find the stress intensification ($\sigma_{1max}/\sigma_y$) at the applied load. The cleavage fracture stress ($\sigma_F$) is then equal to this maximum principal tensile stress ($\sigma_{1max}$).

Fig. 6 is another plot of stress intensification ($\sigma_{1max}/\sigma_y$) vs. the distance below the notch (expressed as multiples of the notch root radius r) as a function of the ratio of the nominal stress to the yield strength ($\sigma_{nom}/\sigma_y$). It is evident from Fig. 6 that as the peak stress increases, its location shifts into the interior of the uncracked ligament away from the

notch root. The maximum possible stress intensification ($\sigma_{1max}/\sigma_y \approx 2.62$) according to this analysis, corresponds to $\sigma_{nom}/\sigma_y \approx 2.2$ when fracture coincides with general yield. An attempt was therefore made to select the test temperatures such that the yield strength of the materials was high enough to prevent general yielding before fracture. Even so, if the ratio of the nominal stress to the yield strength ($\sigma_{nom}/\sigma_y$) exceeded 2.2, an approximate cleavage fracture stress ($\sigma_F$) was estimated at the maximum possible stress intensification $\sigma_{1max}/\sigma_y \approx 2.62$. The yield strengths used in the above mentioned calculations were taken from previous work on similar materials at equivalent strain rates and temperatures [7], in addition to conducting tests on sections taken from the ends of the broken bend bars.

The results of the notch bend testing are shown in Fig. 7. It is shown that the cleavage fracture stress is relatively independant of temperature for both the coarse grained pure Nb and Nb-(ss)Zr samples. The fine grained Nb-(ss)Zr material shows a slight dependence of cleavage fracture stress on the test temperature, in the range tested. The data shows a strong dependance of cleavage fracture stress on the grain size, in agreement with such previous work on steels, while SEM fractography conducted to determine the site(s) of fracture nucleation has been successful(11) and illustrates that the apparent cleavage fracture initiation sites often occur at or near the location of peak tensile stress. Additional discussion of these points is provided elsewhere (11).
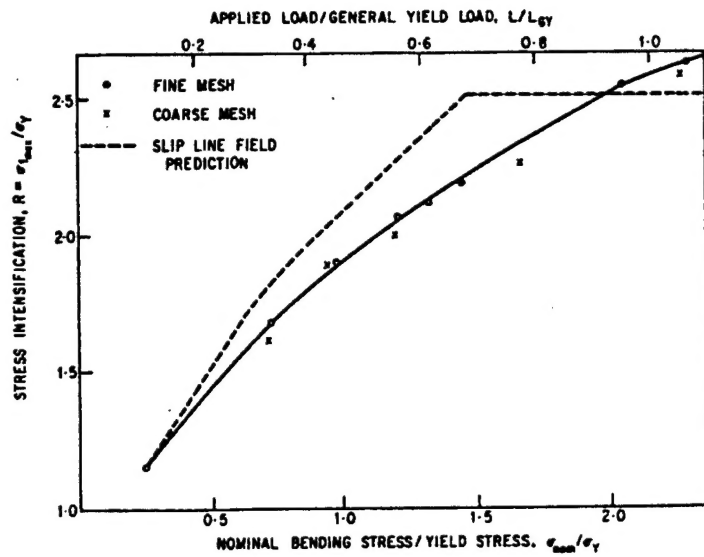
Fig. 5 The variation of stress intensification ($\sigma_{1max}/\sigma_y$) with applied load [10].
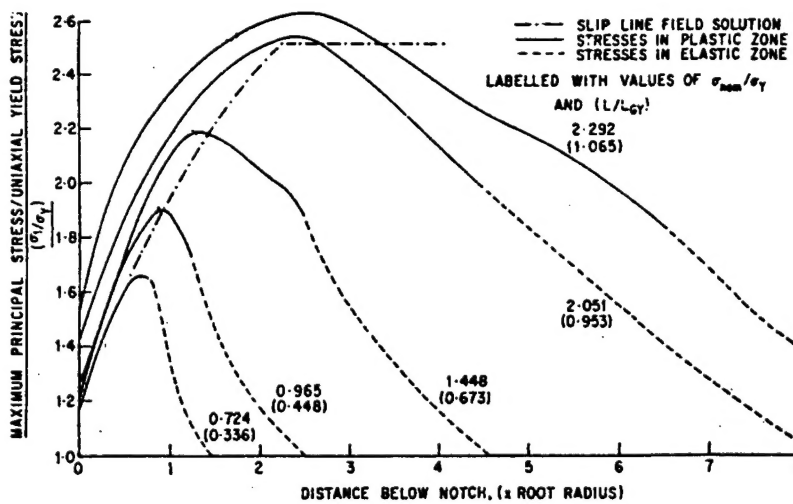


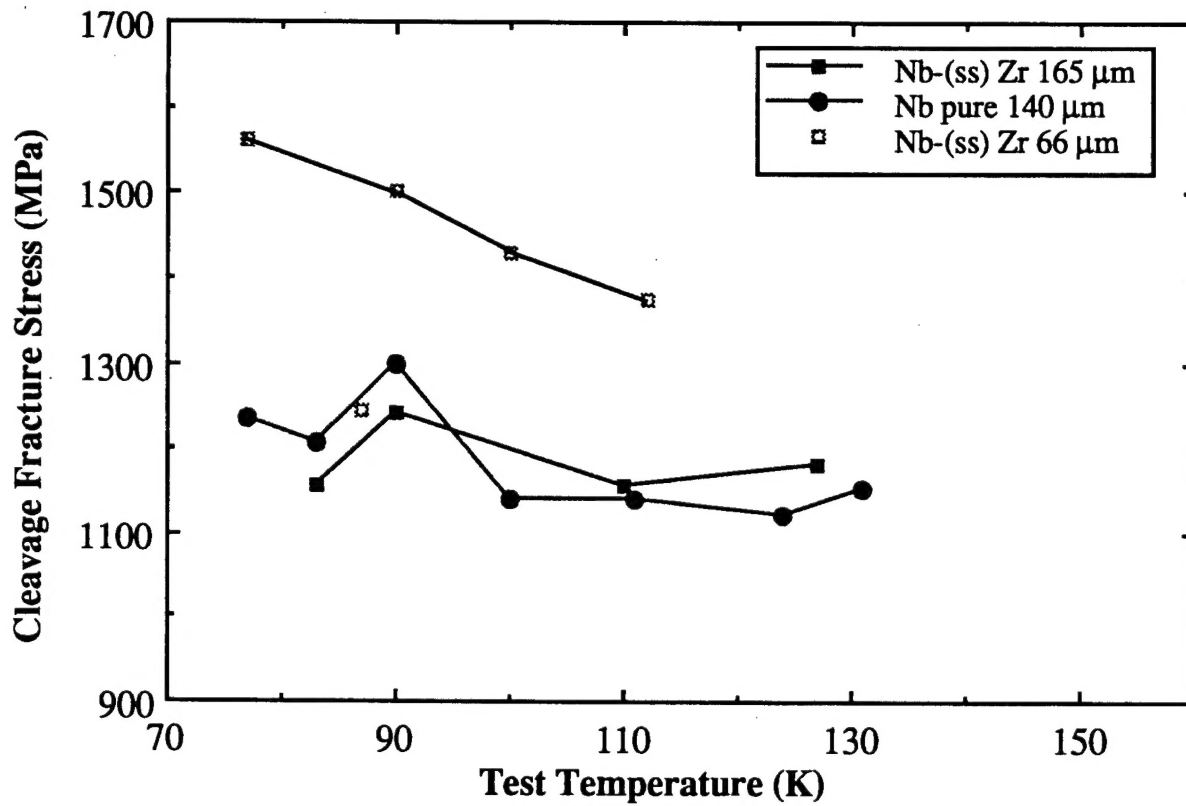Fig. 6 The variation of the maximum principal stress below the notch at various loads [10].

Fig.7 Cleavage fracture stress as a function of test temperature.

# References

1. E. Orowan,*Trans. Inst. Engrs. Shipbuilders Scot.*, **89**, 165, (1945).
2. J.F. Knott,*Fundamentals of Fracture Mechanics*, Butterworths, London, (1973).
3. J.J. Lewandowski,*In-Situ Composites*, M. Singh and D. Lewis, eds.TMS, Warrendale, PA, 159, (1994).
4. J.J. Lewandowski and A.W. Thompson, *Metall. Trans. A*, **17A**, 1769, (1986).
5. J.J. Lewandowski and A.W. Thompson, *Acta Metall.*, **35**, 1453, (1987).
6. R.O. Ritchie, J.F. Knott, and J.R. Rice,*J. Mech. Phys. Solids*, **21**, 395, (1973).
7. J. D. Rigney, *Ph.D. Dissertation*, Case Western Reserve University, 1994.
8. "Standard Test Method for Plain Strain Fracture Toughness of Metallic Materials", ASTM Standard E399-83 in Annual Book of ASTM Standards, Vol. 03.01, American Society for Testing and Materials, Philadelphia, PA, 480 (1988).
9. Y. Murakami, *Stress Intensity Factors Handbook*, 1st Edition, Permagon, New York (1987).
10. J. R. Griffiths and D. R. J. Owen, "An Elastic-Plastic Stress Analysis for a Notched Bar in Plane Strain Bending", *J. Mech. Phys. Solids.*, **19**, 419 (1971).
11. A. Samant and J.J. Lewandowski, *Metall Trans. A,* in review, (1996).